Persistent Spectral Hole-Burning Phenomena in CuCl Nanocrystals

Shinji OKAMOTO

A dissertation submitted to the Doctoral Program
in Physics, the University of Tsukuba
in partial fulfillment of the requirements for
the degree of Doctor of Philosophy (Science)

January, 1997

Abstract

We have studied persistent spectral hole-burning (PSHB) phenomena of cuprous halide (CuCl) nanocrystals. In particular, we concentrate on two aspects: Fundamental physics and applications of the PSHB phenomena.

Stark effects by trapped carriers or photoionization were proposed as the mechanisms of the PSHB phenomena. However, the further study is needed for the better understanding of the mechanism. In the course of the study to this direction, we found correlations between the PSHB phenomena and photoluminescence spectral-changes of excitons bound to Cu^+-ion vacancies in CuCl nanocrystals and of Cu^+ dimers in a NaCl crystal in CuCl nanocrystals embedded in a NaCl crystal. The spectral-changes can be triggered by Cu^+-ion displacements in CuCl nanocrystals and in a NaCl crystal. On the other hand, in CuCl nanocrystals embedded in aluminoborosilicate glass, the PSHB phenomena are considered to be caused by photophysical mechanisms, *e. g.*, photoinduced structural-change at nanocrystal-glass interface and/or glass.

PSHB phenomena can be applied to not only optical memory but also the precise, high-resolution spectroscopy for the nanocrystals with a certain size. We report the nanocrystal-size dependent acoustic phonons confined in CuCl nanocrystals by using the PSHB phenomena. The size-dependent energy-intervals between zero-phonon lines and phonon sidebands in the hole-burning spectra almost coincide with the calculated energies of confined acoustic phonons in nanometer-size elastic spheres. We conclude that the phonon sidebands are due to confined acoustic phonons in CuCl nanocrystals. The observed confined acoustic

phonon mode depends on the elastic constants of the surrounding matrices, glass and NaCl.

Next, we show the nanocrystal-size-dependence of the higher-excited states of $Z_{1,2}$- and Z_3-excitons and LO- and TO-phonons confined in CuCl nanocrystals by means of the PSHB phenomena. Quantum confined exciton excited states were observed and in agreement with the theoretical results on the exciton confinement.

The PSHB phenomena of the nanocrystal systems can be applied to optical data storage devices. Here, we demonstrate frequency-domain optical data storage by using CuCl nanocrystals.

We exhibit possible mechanisms and applications of the PSHB phenomena in CuCl nanocrystals.

Table of Contents

Chapter I

Introduction

In the last decade, semiconductor nanocrystals have attracted considerable attention because of their unique properties [1,2]. Simultaneously, the nanocrystals have possibilities of applications to nonlinear optical devices. For the investigation of the size dependent properties of nanocrystals, it is ideal to fabricate a well-defined single-size of nanocrystals. However, the size distribution of nanocrystals is difficult to be controlled, so that the samples have size distribution and then the absorption band is inhomogeneously broadened [1,2].

Hole-burning spectroscopy is a powerful tool to extract individual and intrinsic information of a certain-sized nanocrystals from the inhomogeneously broadened absorption band. This is because the nanocrystal size decides the energy of photoexcited carriers in the nanocrystals in terms of "quantum confinement effects". Thus, the nanocrystals with a certain size is selectively excited. Then, the hole-burning phenomena in the nanocrystal systems were believed to be caused by absorption saturation of photoexcited carriers, so that the hole burning in direct and allowed semiconductor quantum dots was expected to disappear within a few nanosecond.

Recently, however, there have been many reports on persistent spectral hole-burning (PSHB), long-lived hole-burning or photoinduced absorption-spectral change phenomena of various semiconductor nanocrystals [3]. The spectral holes persist from more than a few microseconds to several hours. Thus, understanding of the mechanism of the PSHB phenomena is needed but still poor: the PSHB phenomena were considered to be caused by

carrier trapping or photochemical reactions. However, the further study is needed for understanding of the mechanism.

A possible application of the PSHB is to precise, high-resolution spectroscopy under the site-selective excitation [4]. This serves as precise investigation of quantum confinement states of the nanocrystals of a certain size. Simultaneously, the PSHB opens up the possibility of new applications of the nanocrystal systems to optical data storage devices [4,5]. Thus, we need search for the possibilities of the applications.

In this thesis, we have investigated the PSHB phenomena of CuCl nanocrystals and discussed two aspects: Fundamental physics and applications of the PSHB phenomena. The content of this thesis is described briefly as follows.

In **Chapter II**, we explain fundamental physics of PSHB phenomena. This includes concepts of two-level-system (TLS) model. On the basis of the TLS model, the spectral-hole growth-rate and thermal-annealing hole-filling are discussed.

In **Chapter III**, we describe properties of CuCl and quantum confinement effects in CuCl nanocrystals. Exciton binding energy in bulk CuCl is large. In case of CuCl nanocrystals, Bohr radius of the excitons is smaller than a typical size of nanocrystals, so that the exciton center-of-mass translational motion is quantized (weak confinement regime).

In **Chapter IV**, we explain sample preparation methods and the experimental setup. We used CuCl nanocrystals in different matrices: NaCl crystals and aluminoborosilicate glass. Moreover, we mention experimental setups briefly.

In **Chapter V**, we discuss the PSHB phenomena of CuCl nanocrystals. In case of CuCl nanocrystals embedded in a NaCl nanocrystals, we found correlations between the PSHB

phenomena and photoluminescence (PL) spectral-changes of excitons in CuCl nanocrystals and Cu^+ dimers in NaCl crystals. The spectral-changes can be triggered by Cu^+-ion displacements in CuCl nanocrystals and NaCl crystals. *Ab initio* calculations of the potential barrier heights for the Cu^+-ion displacements supports this interpretation. In case of CuCl nanocrystals embedded in glass, the PSHB phenomena are considered to be caused by photophysical mechanisms, *e. g.*, photoinduced structural changes of the nanocrystals and/or glass, similar to dye molecules embedded in amorphous materials.

In **Chapter VI**, we discuss the possibility of the applications of the PSHB phenomena. The PSHB phenomena of nanocrystals gives us two possible applications: site-selective spectroscopy and optical memory. We exhibit size-dependent acoustic phonons and excited states of excitons confined in CuCl nanocrystals by using the PSHB phenomena. Moreover, we demonstrate the frequency-domain optical data storage by using CuCl nanocrystals embedded in a NaCl crystal and in glass. For the application, we must find out the PSHB materials with a large Debye-Waller factor at high temperature [6]. CuCl nanocrystal systems are found to maintain the spectral holes at high temperature up to 150 K [7] and have the large Debye-Waller factor which is larger than 0.5 [8]. Thus, CuCl nanocrystals are candidates for high temperature PSHB materials.

In **Chapter VII**, we conclude this thesis.

References

[1] A. I. Ekimov, Al. L. Efros and A. A. Onushchenko, Solid State Commun. **56**, 921 (1985).

[2] L. Brus, IEEE. J. Quantum Electron. **QE-22**, 1909 (1986).

[3] Y. Masumoto, L. G. Zimin, K. Naoe, S. Okamoto, T. Kawazoe and T. Yamamoto, J. Lumin. **64**, 213 (1995) and references therein.

[4] *Persistent Spectral Hole-Burning: Science and Applications,* edited by W. E. Moerner (Springer-Verlag, Berlin, Heidelberg, 1988).

[5] A. Szabo, U. S. Patent No. 3,896,420 (1975).

[6] S. Saikan, A. Imaoka, Y. Kanematsu, K. Sakoda, K. Kominami and M. Iwamoto, Phys. Rev. B**41** 3185 (1990).

[7] S. Okamoto and Y. Masumoto, Jpn. J. Appl. Phys. **34** Suppl. 34-1, 128 (1995).

[8] S. Okamoto and Y. Masumoto, J. Lumin **64**, 253 (1995).

Chapter II

Persistent Spectral Hole-Burning (PSHB) Phenomena

Spectral hole-burning is a well-known phenomenon used for the measurement of the homogeneous linewidth Γ_h in inhomogeneous linewidth Γ_i. A intense pump pulse causes bleaching, that is absorption saturation, in the absorption spectrum, and the change in the spectrum is detected by the much weaker probe pulse. If the pump pulse has the sufficiently narrow linewidth, the saturation occurs within the energy range Γ_h around the pump laser energy E_p. The pump photon energy selects a certain sized nanocrystals. In this sense, we can call this method the size-selective excitation on the analogy of the site-selective excitation. Thus, a hole, whose width is Γ_h, is burnt out in the absorption profile. Using this spectroscopy, we can measure the optical properties of a size-selected nanocrystal. The photoexcited carriers have a lifetime of a few nanoseconds in direct and allowed semiconductor quantum dots. The spectral holes are believed to disappear within a few nanoseconds since the holes come from absorption saturation of photoexcited carriers. However, there are many reports on the persistent or long-lived spectral-holes [1].

Persistent spectral hole-burning (PSHB) is a process whereby the spectrally narrow hole in the inhomogeneously broadened absorption band in solids is preserved for time periods longer than the lifetime of any excited state [2]. The PSHB spectroscopy is a powerful tool to investigate impurities in solids and can be used to study dephasing mechanisms and local-environments of a host. Simultaneously, the PSHB has the potential for technological applications to optical data storage and optical signal processing [2,3]. This brings forth a lot

of researches on PSHB around the world. PSHB had been observed in dye molecules in glass and polymer, rare-earth ions in amorphous material, etc.

The basic requirements for PSHB phenomena are as follows:

(1) the optical absorption of guests, *e. g.*, nanocrystals, molecules, etc., must be inhomogeneously broadened;

(2) the photoexcitation changes the guest themselves, and/or the environments around the guests, and then the absorption lines of the guests are changed, *e. g.*, the transition energy shifts, and;

(3) the relaxation among the ground states must be slower than the decay rate of any excited state.

The requirements may seem restrictive, but many examples of PSHB show that PSHB is observed widely in solids at low temperatures.

In this chapter, we outline fundamental physics of the PSHB systems needed for analysis of the experimental results: two-level-system (TLS) model, time evolution of hole depth, and temperature-cycling hole-filling.

2.1 Two-Level-System (TLS) Model

PSHB phenomena can be well-explained by a two-level-system (TLS) model. Concept of the TLS model was proposed by Anderson *et al.* [4] and Philips [5] to explain the specific heat dynamics of amorphous materials.

Figure 2.1 shows the schematic of the TLS system. The sequence of the species motion in the TLS systems is as follows:

(1) resonant excitation in an absorption site by using a narrow-band laser;

(2) site relaxation due to a tunneling process;

(3) relaxation to the ground state in the other absorption site, and;

(4) at low temperature, the species do not return to its original absorption site.

Thus, the absorption lines irradiated is reduced, *i. e.*, a "spectral-hole" is created, and then the other absorption lines are increased and/or new absorption lines are created, *i. e.*, "photoproducts" are created [2].

The time evolution of the hole depth and the temperature-cycling hole-filling is based on the TLS model.

2.2 Time Evolution of Hole Depth

The hole depth exhibits logarithmic time dependence with saturation. The nonexponential time-evolution of the hole depth is explained by a model on the assumption of the broadly distributed TLS with various distance and depth. Following Ref. 6, the hole-burning rate constant K is expressed by $K = K_T \exp(-\lambda)$, when we suppose that the distribution of λ is Gaussian with standard deviation σ and center λ_0. Since the burning reaction is considered to occur via a tunneling through potential barriers in the excited state between the TLS, λ represents a tunneling parameter of the form $\lambda = d(2mV)^{1/2}/h$, where d is the tunneling distance, m is the mass of the tunneling species and V is the barrier height.

The time evolution of normalized concentration of species, *i. e.*, normalized hole-depth, is well expressed by

$$M(t) = \frac{1}{(2\pi\sigma)^{1/2}} \int_{-\infty}^{+\infty} \exp\{-\frac{(\Delta\lambda)^2}{2\sigma^2} - K_T\, t\, \exp[\, -(\lambda_0 + \Delta\lambda)]\}\, d(\Delta\lambda)\ , \qquad (2.1)$$

where t represents the exposure time, and λ_0 the center of the distribution.

2.3 Temperature-Cycling Hole-Filling

The theory of thermal erasing of the spectral holes is also based on the TLS model. The experiment sequence is as follows. At first, holes are burned at certain temperature T_b and the hole area is measured. After cycling through the elevated temperature T, the hole area is measured again at T_b. This experiment is the so-called temperature-cycling experiment. The reduction of hole area by means of the temperature-cycling is explained generally by the model proposed in Ref. 7. This model is assumed that the burned hole is filled via thermally activated barrier crossing over the barrier height V and the distribution function of V is proportional to $1/\sqrt{V}$. The $1/\sqrt{V}$- dependent distribution function may reflect the hierarchy of the TLS systems, such as amorphous systems [7].

Then, the normalized hole area is expressed by

$$\frac{A(T)}{A_0} = \frac{1-(\alpha kT/V_{0\max})^{1/2}}{1-(\alpha kT_b/V_{0\max})^{1/2}}\ , \qquad (2.2)$$

where A_0 and $A(T)$ are the initial hole area and the hole area after heat cycling, respectively. The parameter α is defined by $\ln(\nu_0 t)$, where ν_0 is the attempt frequency and t is the time for which the sample has been maintained at temperature T. $V_{0\max}$ is a maximum barrier height.

References

[1] Y. Masumoto, L. G. Zimin, K. Naoe, S. Okamoto, T. Kawazoe and T. Yamamoto, J. Lumin. **64**, 213 (1995) and references therein.

[2] *Persistent Spectral Hole-Burning: Science and Applications*, edited by W. E. Moerner, (Springer-Verlag, Berlin, 1988).

[3] A. Szabo, U. S. Patent No. 3,896,420 (1975).

[4] P. W. Anderson, B. I. Halperin and C. M. Varma, Phil. Mag. **25**, 1 (1972).

[5] W. A. Philips, J. Low Temp. Phys. **7**, 351 (1972).

[6] R. Jankowiak, R. Richert and H. Bässler, J. Phys. Chem. **89**, 4569 (1985).

[7] W. Köhler, J. Meiler and J. Friedrich, Phys. Rev. B**35**, 4031 (1987).

Figure Captions

Fig. 2.1. Two-level-system (TLS) represented in a configurational coordinate model by a double-well potential. V and d denote barrier height and distance between two minima, respectively.

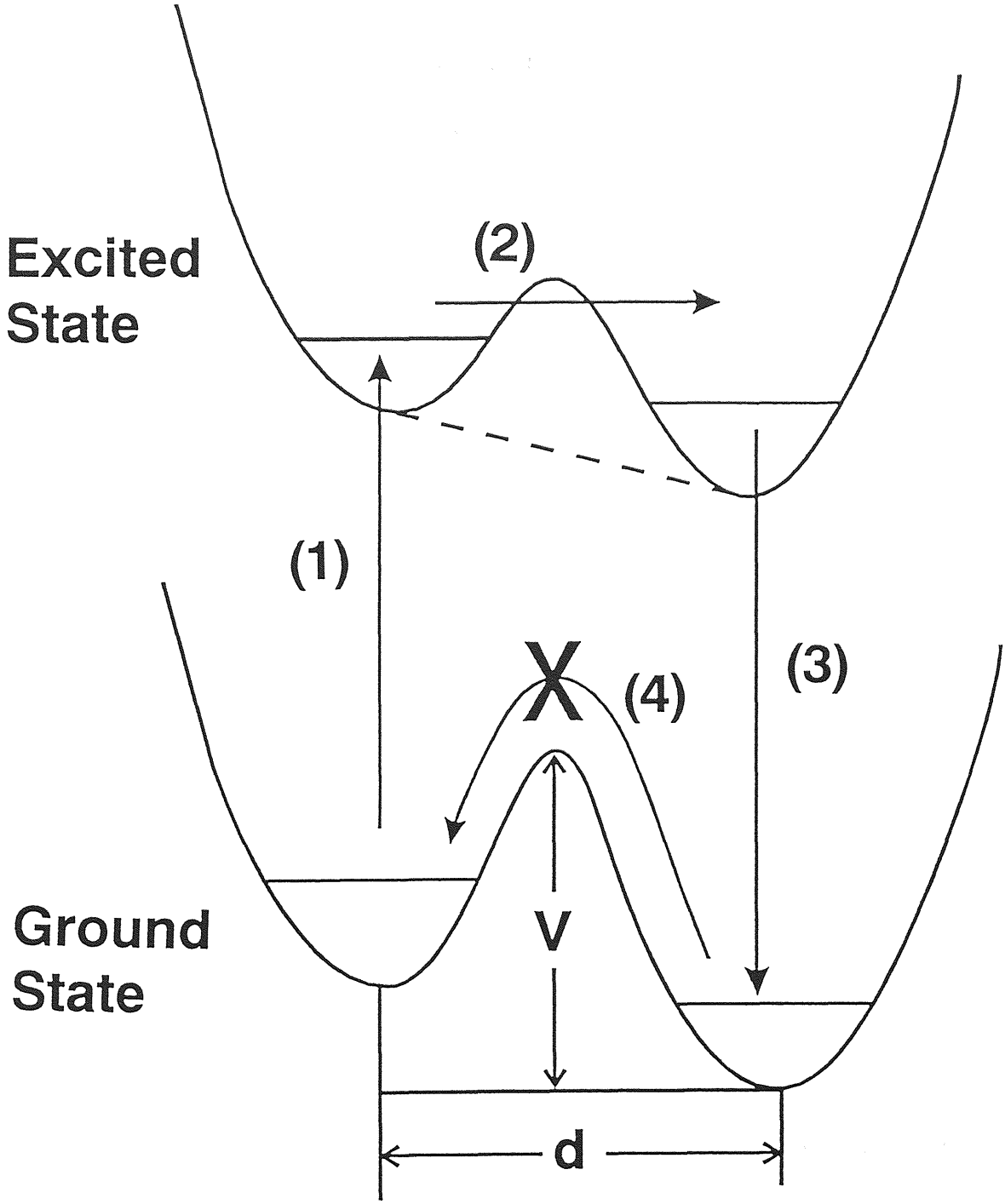

Fig. 2.1

Chapter III

CuCl Nanocrystals

In this chapter, we outline properties of bulk CuCl and quantum confinement effects on CuCl nanocrystals.

3.1 Properties of Bulk Cuprous Chloride (CuCl)

Cuprous chloride (CuCl) is a direct wide-gap semiconductor with zinc-blende structure below 660 K. The band-gap energy is 3.396 eV at 4.2 K [1]. The top of the valence-band at Γ point is separated into two bands, Γ_7 and Γ_8, due to spin-orbit coupling. The Wannier-type excitons consisting of holes of Γ_7 and Γ_8 are called $Z_{1,2}$-excitons and Z_3-excitons, respectively. The excitons exist stably at low temperature because of their large binding energy of 120 meV for $Z_{1,2}$-exciton and 190 meV for Z_3-exciton at 4.2 K. The absorption lines of the excitons are in the ultraviolet region.

Two Z_3-excitons are bounded together stably to form a biexciton at low temperature when excitons are produced with high density in CuCl bulk crystals by intense light. Biexciton binding energy is 32 meV [1], and when radiative decay of biexcitons occurs, the nonlinear luminescence band, M-band, appears at the low-energy side of Z_3-exciton luminescence band. The binding energies of the excitons and biexciton in CuCl are very large.

3.2 Quantum Confinement Effects in CuCl Nanocrystals: Weak Confinement Regime

A nanocrystal in a host matrix can be treated as a three-dimensional potential well for particles such as electrons, holes, excitons and biexcitons. These particles are allowed to have discrete values for energy because there are only limited space for these particles to move. The energy quantization is so-called "quantum confinement effects". The effects cause a blue shift, *i. e.*, a shift to the higher-energy side of the absorption and the luminescence spectra.

The quantum confinement effect strongly depends on the Coulomb interaction of electrons and holes. It is assumed that nanocrystals are spherical with infinite potential barriers at nanocrystal-host matrix interface and the energy bands are parabolic (effective-mass approximation). Applying the effective-mass approximation, the quantum confinement effects are classified as [2,3]

$a_{ex} \gg a$: strong confinement (electron-hole individual confinement);

$a_{ex} \approx a$: medium confinement;

$a_{ex} \ll a$: weak confinement (exciton confinement);

where a_{ex} is the effective Bohr radius of exciton in the single crystal and a is the radius of nanocrystals. In case of CuCl nanocrystals, the exciton center-of-mass translational motion is quantized since the exciton Bohr radius (0.7 nm) is smaller than typical size of nanocrystals (>1 nm). The blue shift of the exciton energy is well expressed by [4]

$$\Delta E_{ex} = \frac{\hbar^2 \pi^2}{2 M_{ex} (a - \frac{a_{ex}}{2})^2} , \tag{3.1}$$

where M_{ex} is the translational mass of exciton, $\hbar$ is Planck's constant divided by 2π, a is the

radius of nanocrystals and a_{ex} is the Bohr radius of the exciton. Here the so-called dead layer correction is included as a form of $a-a_{ex}/2$.

References

[1] *Physics of II-VI and I-VII Compounds, Semimagnetic Semiconductors*, edited by O. Madelung, M. Schulz and H. Weiss, Landolt-Börnstein, New Series, Group III, Vol. 17, Pt. b (Springer-Verlag, Berlin, 1982).

[2] A. I. Ekimov, Al. L. Efros and A. A. Onushchenko, Solid State Commun. **56**, 921 (1985).

[3] A. D. Yoffe, Adv. Phys. **42**, 173 (1993).

[4] T. Itoh, Y. Iwabuchi and M. Kataoka, Phys. Status Solidi B**145**, 567 (1988).

Chapter IV

Experimental

In this chapter, we briefly mention sample preparation procedures of CuCl nanocrystals embedded in NaCl crystals and in glass. We also describe experimental setup of spectral hole-burning measurements.

4.1 Sample Preparation

Samples investigated here were CuCl nanocrystals embedded in NaCl crystals and in aluminoborosilicate glass. The detailed sample preparation methods were described in Refs. 1-3. Here, we will mention them briefly.

Samples of CuCl nanocrystals embedded in NaCl host crystals were made from a mixture of pure NaCl powder and CuCl powder of 1 mol% in concentration. The mixture was sealed in a quartz ampule in vacuum, and the doped crystals were grown in a transverse Bridgman furnace. The as-grown crystals were cleaved into several pieces and annealed in vacuum or an argon atmosphere in order to change the size distribution of CuCl nanocrystals [2]. We usually annealed the samples twice: At the first heat treatment, Cu^+ ions in the as-grown samples are dispersed. At the second heat treatment, the dispersed Cu^+-ions thermalaggregate, as a result, CuCl nanocrystals are fabricated via supersaturated solid-solution [2,3]. The second anneal temperature and time control the average size of the nanocrystals.

Samples of CuCl nanocrystals embedded in glass were made from a mixture of raw

material powder of silicate glass and CuCl powder of 1 mol%. The mixture was dissolved in a crucible. At the secondary heat treatment of the glass samples, nucleation and growth of the nanocrystals occurs as a result of a diffusive phase decomposition of the supersaturated solid solution [1]. The composition of the glass used in this investigation is as follows; SiO_2: 63.5, B_2O_3: 32.9, Al_2O_3: 1.8, P_2O_5: 0.5, CuCl: 0.5, K_2O: 0.4, Sb_2O_3: 0.4, in a unit of mol%.

The mean radii of the prepared samples were determined by using small-angle x-ray scattering measurements. The results are almost consistent with estimations from blueshift of the absorption band by using a simple quantum confinement model [2].

4.2 Experimental Setup

The equipment setup for persistent spectral-change is displayed by Fig. 4.1. A narrow-linewidth dye laser was used in the hole-burning experiments. For the site-selective excitation, a dye laser (HD-500; Lumonics) pumped by the third harmonics of the output of a Q-switched Nd^{3+}: YAG laser (GCR-3; Spectra Physics) was used as a pump source. The active medium of the dye laser was Exalite 384 or 389. The spectral width was 0.014 meV. For band-to-band excitation, the third harmonics of the output of a Q-switched Nd^{3+}: YAG laser (GCR-3; Spectra Physics) was used as a pump source. The pulse duration of these laser was 5 ns and the pulse repetition rate was 30 Hz. We used a halogen lamp to investigate transmittance spectra before and after the laser exposure. The transmittance and photoluminescence signals were dispersed by a 25-cm monochromator (CT-25CP; JASCO) or a 93-cm monochromator (SPEX 1702). The dispersed signals were detected by a diode-array-type optical-multichannel-analyzer (OMA; EG&G PARC) or liquid nitrogen cooled

charge-coupled-device (CCD; Princeton Instruments Inc.). The absorption-change spectra (hole spectra) are defined as the difference of the absorption spectra taken before and after the sample is exposed to the laser light.

For the confined-acoustic-phonon measurements mentioned in Sec. 6.1, we adopted a nanosecond (quasi steady-state) pump-and-probe method in order to avoid the large spectral-change of absorption. The equipment setup for transient spectral-change is displayed by Fig. 4.2. Similar setup was used as the measurements of homogeneous linewidth [4]. A dye laser (HD-500; Lumonics) pumped by the third harmonics of the output of a Q-switched Nd^{3+}:YAG laser (GCR-3; Spectra Physics) was used as a pump source. The active medium of the dye laser was Exalite 384 or 389. The spectral width was 0.014 meV. As a probe source, amplified spontaneous emission (ASE) from LD 390 dye solution excited by a portion of the third harmonics of the output of the Q-switched Nd^{3+}:YAG laser was used. The time delay between the pump and probe pulses was adjusted to be zero and the polarizations of the pump and probe beams were set to be perpendicular to each other. The probe beam was focused on the sample onto a spot which lay inside a spot of the pump beam. The probe beam through the sample was analyzed by a 93-cm monochromator in conjunction with an OMA.

In the pump-and probe experiments, the change in absorption can be measured and expressed as the form of differential absorption spectrum. The differential absorption spectrum, $-\Delta\alpha d$, is defined as

$$
\begin{aligned}
-\Delta\alpha d &= (\alpha d)_0 - (\alpha d)_{PUMP} \\
&= -\ln \frac{I_{PROBE}}{I_{REF}} - \left[-\ln \frac{I_{P.P} - I_{PUMP}}{I_{REF}} \right] \\
&= -\ln \frac{I_{PROBE}}{I_{P.P} - I_{PUMP}}
\end{aligned}
\quad , \qquad (4.1)
$$

where $(\alpha d)_0$–$(\alpha d)_{\mathrm{PUMP}}$ represents absorbance of the sample without and with a pump beam, respectively; I_{REF} the intensity of the probe beam; I_{PROBE} and $I_{\mathrm{P.P}}$ the measured transmitted intensity of the probe beam through the sample without and with a pump beam, respectively; I_{PUMP} the intensity of pump–beam scattering and photoluminescence. Since the pump intensity is much larger than the probe intensity, $I_{\mathrm{P.P}}$ involves the effects of pump–beam scattering and photoluminescence. Therefore, we omit them by subtracting I_{PUMP} from $I_{\mathrm{P.P}}$, as shown in Eq. 4.1. We neglect the intensity profile of the pump laser in the samples. The experimental sequence is as follows: The accumulated data of I_{PROBE}, $I_{\mathrm{P.P}}$ and I_{PUMP} were individually measured in that order, and then the differential absorption spectra were calculated by using Eq. 4.1.

The samples were immersed in superfluid liquid helium or mounted on the cold finger of a temperature–variable cryostat.

References

[1] A. I. Ekimov, Al. L. Efros and A. A. Onushchenko, Soild State Commun. **56**, 921 (1996), and references therein.

[2] T. Itoh, Y. Iwabuchi and M. Kataoka, Phys. Status Solidi B**145**, 567 (1988).

[3] Y. Masumoto, M. Yamazaki and H. Sugawara, Appl. Phys. Lett. **53**, 1527 (1988).

[4] T. Wamura, Y. Masumoto and T. Kawamura, Appl. Phys. Lett. **59**, 1758 (1991).

Figure Captions

Fig. 4.1. Experimental setup for observation of persistent spectral hole-burning phenomena.

Fig. 4.2. Experimental setup for observation of nanosecond spectral hole-burning phenomena.

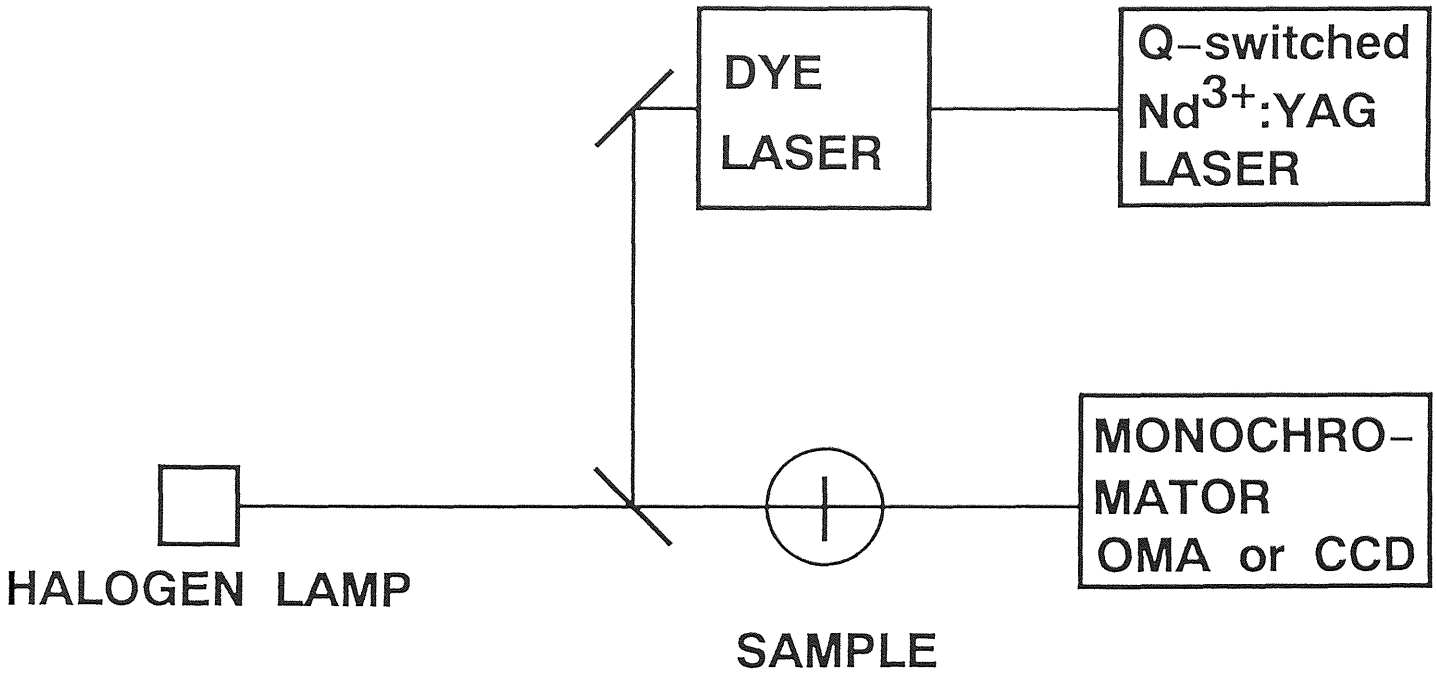
DYE
LASER
Q-switched
Nd3+:YAG
LASER
MONOCHRO-
MATOR
OMA or CCD
HALOGEN LAMP
SAMPLE

Fig. 4.1

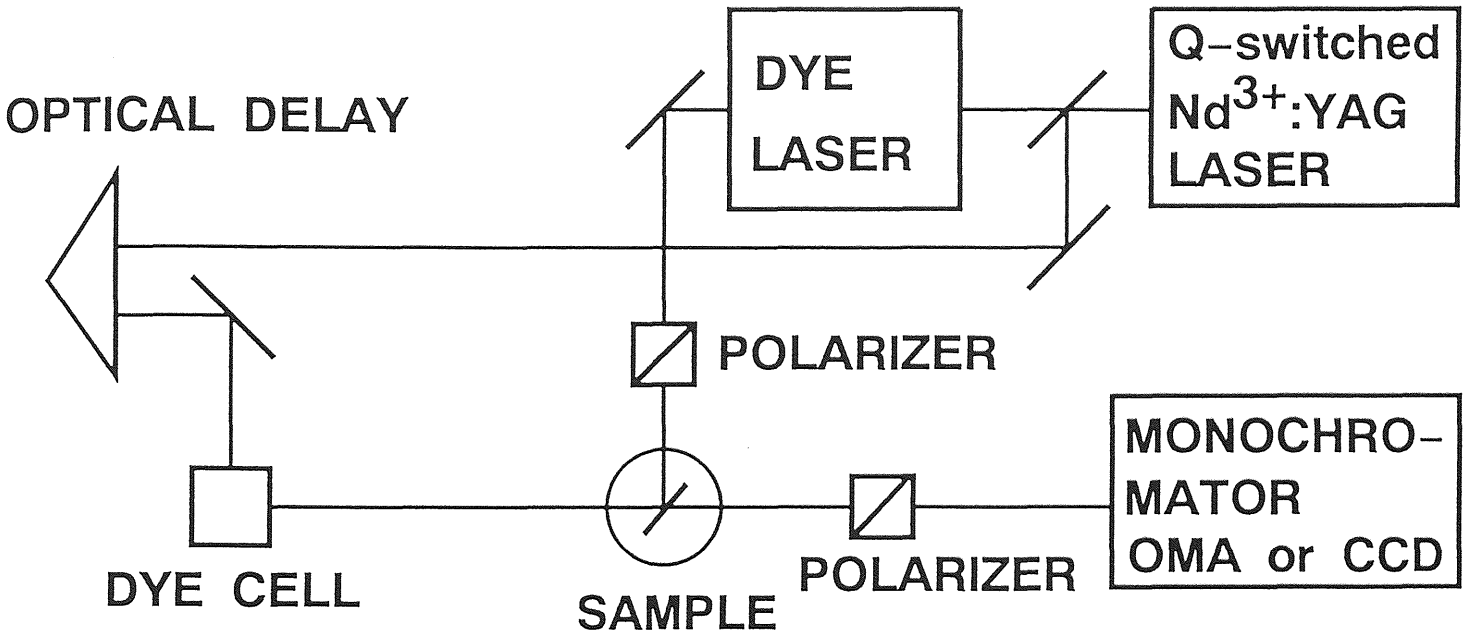
OPTICAL DELAY
DYE
LASER
Q-switched
Nd3+:YAG
LASER
POLARIZER
MONOCHRO-
MATOR
OMA or CCD
DYE CELL
SAMPLE
POLARIZER

Fig. 4.2

Chapter V

Persistent Spectral Hole-Burning (PSHB) in CuCl Nanocrystals

Recently, there have been many reports on persistent spectral hole-burning (PSHB), long-lived hole-burning or photoinduced absorption-spectral change phenomena of various semiconductor nanocrystals [1]. However, the mechanisms of the PSHB phenomena are poorly understood. A few mechanism are proposed: carrier trapping or photochemical reactions. However, The further study is necessary for the understanding of the mechanism.

In this chapter, we present experimental results of persistent spectral hole-burning (PSHB) phenomena of CuCl nanocrystals embedded in different matrices: a NaCl crystal and aluminoborosilicate glass. We discuss possible mechanisms of the PSHB phenomena and the matrix-dependence on the mechanisms.

5.1 CuCl Nanocrystals Embedded in NaCl Crystals

In this section, we have investigated the PSHB phenomena of CuCl nanocrystals embedded in NaCl crystals by using the laser-induced spectral-change and temperature-cycle experiments. The experimental results show that the PSHB phenomena can be explained by the two-level-system (TLS) model, analogous to dye molecule-glass systems. The results indicate that there are two types of TLS's in the samples. We found correlations between the PSHB phenomena and photoluminescence (PL) spectral-changes of excitons in CuCl nanocrystals and Cu^+ dimers in NaCl crystals: the absorption and PL spectra are simultaneously modified with an increase of the laser irradiation, and recover at the same

cycling temperatures. The spectral-changes can be triggered by Cu^+-ion displacements in CuCl nanocrystals and NaCl crystals. *Ab initio* calculations of the potential barrier heights for the Cu^+-ion displacements supports this interpretation.

5.1.1 Demonstration of PSHB Phenomena in CuCl Nanocrystals Embedded in NaCl Crystals

Figure 5.1.1 (a) shows absorption spectra of CuCl nanocrystals embedded in a NaCl crystal at 2 K. The dash-dotted line in Fig. 5.1.1 (a) represents the spectrum before the dye laser irradiation. The Z_3-exciton absorption band is inhomogeneously broadened, and shows the blueshift from its position in bulk CuCl. The blueshift is 16 meV. The mean radius of the nanocrystals estimated from the blue shifts on the exciton quantum confinement model [2] is almost consistent with the SAXS results. The absorption spectrum is changed after the dye laser exposure, as indicated by a solid line in Fig. 5.1.1 (a). Figure 5.1.1 (b) displays the absorption-spectral change of the sample. The hole spectra were recorded at 2 min (a dashed line) and at 20 min (a solid line) after the laser exposure was stopped. The spectral holes are preserved for more than 20 min, much longer than the exciton lifetime [1]. Further, we confirmed the persistency of the holes for several hours. The hole spectrum is more complicated than that of CuCl nanocrystals embedded in glass [1]: The main spectral-holes are superposed on the large wavy structures coming from the redshift-like spectral change of the absorption band. Satellite holes are also clearly observed: the solid circle in Fig. 5.1.1 (b) indicates the main hole; the open triangle the LO-phonon sideband; the solid triangle the TO-phonon sideband; the open square the sideband of TA-phonon at the Brillouin-zone edge; the

solid square sideband of the $Z_{1,2}$-excitons.

5.1.2 Laser-Exposure-Time Evolution of Hole-Depth

The hole depth grows nearly in proportion to the logarithm of the laser exposure time, as shown in Fig. 5.1.2. The logarithmic hole growth is due to a broad distribution of the hole-burning rate. Similar hole growth occurs in CuBr and CuI nanocrystals embedded in glass [1,3] and dye-doped organic glass [4] and the color centers in crystals. The PSHB phenomena are considered to take place by tunneling from one site to another through the potential barrier with distributed barrier height and width. The double-well potential model, so-called two-level-system (TLS) model, is used to analyze the hole growth. Fitting the expression given by Ref. 4 to the experimental results (see, Sec. 2.2), we obtained the standard deviation σ=3.5 for the Gaussian distribution of the burning rate. The values of σ are comparable to or a little larger than that of the dye-glass systems [5]. The experimental hole-growth is well reproduced by the calculation.

5.1.3 Temperature-Cycling Hole-Filling

The hole structures are erasable by the temperature rise. Figure 5.1.3 shows (a) absorption spectrum, (b) hole spectra at various cycling temperature, and (c) the hole area plotted as a function of the cycling temperature. This experimental sequence is as follows: At first, the spectral holes are burned at certain temperature T_b, and the hole spectrum is measured; after cycling through the elevated temperature (cycling temperature) T, the hole spectrum is measured again at T_b. The annealing-temperature-dependent hole area have been fitted by the functional form of $(1-\sqrt{kT\ln(\nu_0 t)/V_{0max}})/(1-\sqrt{kT_b\ln(\nu_0 t)/V_{0max}})$ for $kT\ln(\nu_0 t)<V_{0max}$,

in case of dye molecules in organic glass [6]. Here, $\ln(\nu_0 t)$ is the logarithm of the product of the attempt frequency and the annealing time, and is given by 32~35. V_{0max} is the maximum barrier height. This functional form is derived from the thermal activation model across the distributed barrier height. We tried to fit the expression to the experimental results and estimated the maximum barrier height V_{0max} between the TLS. Two components are necessary to account for the data. The maximum barrier height is 140~160 meV for T<50 K and 400~420 meV for T>50 K. The absorption-change spectra abruptly varied after the temperature was elevated above 50 K, as displayed in Fig. 5.1.3 (b): At the cycling temperature above 50 K, the large wavy structures coming from redshift-like spectral-changes almost disappear, and antiholes, *i. e.*, induced absorption adjacent to the spectral hole (open triangles in Fig. 5.1.3 (b)), appear. Antiholes are important sign that the PSHB phenomena are photophysical, *e. g.*, local-environmental changes around the nanocrystals [1]. At the cycling temperature above 150 K, the spectral change almost disappear. These observations prove the coexistence of two kinds of TLS's in the sample.

5.1.4 Discussions: Correlations between the PSHB Phenomena and Photoluminescence Spectral-Change

We found correlations between the absorption spectral-changes showing PSHB phenomena and PL spectral-changes of excitons and Cu^+ dimers. Figure 5.1.4 (a), (b) and (c) show absorption, absorption-change spectra and PL spectra after the laser irradiation with the 3.492-eV excitation energy, respectively. The excitation source was the third harmonics of the output of the Q-switched Nd^{3+}: YAG laser. In the absorption-change spectra, only wavy structures coming from redshift-like spectral-change were observed since the pump

photon energy corresponds to the band-to-band transition. Laser irradiation induces not only absorption-spectral changes but also PL-spectral changes [7]: At first, PL peak was at the Z_3-exciton absorption peak (●). With an increase of the laser irradiation time, another PL peak (×) grew and the absorption spectrum was modified. Here, we note a point: The lowest-energy peak of the absorption-change (○) and the peak of the PL spectra (×) in the well-irradiated sample are at almost the same energy positions and approach to bulk I_1 center, which is ascribed to excitons bound to neutral acceptors made of Cu^+ vacancies in CuCl [8], with the increase of nanocrystal size. This result suggests that the observed peaks originate from I_1 centers, namely Cu^+-ion vacancies in CuCl nanocrystals.

Moreover, we found that the PL spectra as well as absorption-change spectra of excitons change with the increase of cycling temperatures: Above the cycling temperature of 50 K, the absorption spectral-changes, *i. e.*, wavy structures coming from redshift-like absorption-change, almost disappear. This observation is consistent with the abrupt spectral-change observed at 50 K, as shown in Fig. 5.1.3 (b). Simultaneously, the PL spectra returned to the spectra observed before the intense laser irradiation. This can be explained by considering that I_1 centers, namely Cu^+-ion vacancies, were reduced by thermal activation.

PL spectral-changes due to Cu^+-ion displacements are observed not only in CuCl nanocrystals but also in a NaCl crystal. The PL band in Fig. 5.1.5 is ascribed to Cu^+ dimers in a NaCl crystal since the PL lifetime (~50 μs), the band width (~0.2 eV) and the peak position (~2.1 eV) are consistent with those of Cu^+dimers at low temperatures reported in Refs. 9-11. It is reasonable to expect that CuCl nanocrystals are surrounded by Cu^+ dimers since the nanocrystals are formed by aggregation of Cu^+ ions [2,9]. At 25 K, the PL ascribed to Cu^+ dimers decreases its intensity with the increase of the laser irradiation time, as shown

in Fig. 5.1.5 (a). After the PL spectra of the dimers are sufficiently changed by the intense laser irradiation, the PL intensity increases with the increase of the cycling temperature and quickly recover when the cycling temperature exceeds 150 K, as shown in Fig. 5.1.5 (b). These observations can be explained by photodissolution of Cu^+ dimers and thermal aggregation. The phenomena are considered to occur via the ion-exchange between Na^+ and Cu^+ ions, similar to Cu^+ ions in Cu^+-doped Na^+-β''-alumina [10].

The cycling-temperature dependence of recovery of the PL and absorption spectra are correlated with the return movement of Cu^+ ions in CuCl nanocrystals and in a NaCl crystal to the previous sites at the cycling temperature above 50 K and 150 K, respectively. The cycling-temperature dependence of the PL spectral-change due to Cu^+ ions coincides with that of the PSHB phenomena. Here, it should be noted that the potential barrier heights obtained from the temperature-cycling experiments are almost consistent with those for Cu^+-ion displacements in a CuCl and a NaCl crystals by *ab initio* calculations: from the temperature-cycling experiments, potential barrier heights is estimated to be 140-160 meV and 400-420 meV; from *ab initio* calculations, potential barrier heights for Cu^+-ion displacements between on- and off-center sites in bulk CuCl was estimated to be 120 meV [12] and 180 meV [13], and for a formation of a Cu^+ site in NaCl crystals via Na^+-Cu^+ ion-exchange was estimated to be 160-870 meV [14]. Thus, barrier heights of 140-160 meV obtained from the temperature-cycling experiments corresponds to those for Cu^+-ion displacements in CuCl nanocrystals; the barrier heights of 400-420 meV to those for Cu^+-ion displacements in NaCl crystals.

Observed facts suggest the strong correlation between the Cu^+-displacements and the PSHB phenomena. Although we cannot explain the PSHB mechanisms quantitatively, we

speculate a possible PSHB mechanism as follows. Site-selective excitation creates excitons in nanocrystals, and induces two types of Cu^+ displacements: one occurs in CuCl nanocrystals and the other in a NaCl crystal. These processes result in photocreation of I_1 centers in CuCl nanocrystals and photodissolution of Cu^+ dimers in a NaCl crystal. The photocreation of I_1 centers forms new absorption band at lower-energy side of Z_3-exciton absorption band and reduces the Z_3-exciton absorption band. At the same time, the I_1 centers can affect the $Z_{1,2}$-excitons. A new absorption band at the lower-energy side of the $Z_{1,2}$-exciton absorption band is formed, and the $Z_{1,2}$-exciton absorption band is reduced. The creation of new absorption bands and reduction of the exciton absorption bands are possibly an origin of the large wavy structure coming from the redshift-like absorption-change. On the other hand, the photodissolution of Cu^+ dimers to Cu^+ monomers around nanocrystals induces local-environmental changes, *e. g.*, the change of the number of carriers trapped in matrix defects, or/and local-distortional change caused by the Cu^+-Na^+ exchange around the nanocrystals. The environmental changes probably perturb the excitons in nanocrystals and cause the absorption change where the wavy structures turn upside down, as shown in spectrum C in Fig. 5.1.3. Thus, the absorption changes due to the Cu^+-displacements inside and outside of the nanocrystals simultaneously occur under the laser exposure. When the cycling temperature is below 50 K, most of Cu^+ ions in CuCl nanocrystals and a NaCl crystal will not return to the sites before the intense laser irradiation and the spectral changes are preserved. When the cycling temperature is above 50 K, most of Cu^+ ions in CuCl nanocrystals return to the previous sites, and then I_1 centers disappear. On the other hand, Cu^+ ions in a NaCl crystal do not return because the potential barrier is higher. As a result, only the spectral-change attributed to the Cu^+-displacements in a NaCl crystal remains, and then the abrupt spectral-

changes are observed (spectrum C in Fig. 5.1.3 (b)). The spectral change vanishes when the cycling temperature is above 150 K.

5.1.5 Summary

In conclusion, we have reported on the PSHB phenomena of CuCl quantum dots embedded in a NaCl crystal. The experimental results show that the PSHB phenomena can be explained by two types of TLS's. The PSHB and PL spectral-change phenomena can be triggered by photoinduced Cu^+-ion displacements in CuCl and NaCl.

References

[1] Y. Masumoto, L. G. Zimin, K. Naoe, S. Okamoto, T. Kawazoe and T. Yamamoto, J. Lumin. **64**, 213 (1995) and references therein.

[2] T. Itoh, Y. Iwabuchi and M. Kataoka, Phys. Status Solidi B**145** 567 (1988).

[3] Y. Masumoto, K. Kawabata and T. Kawazoe, Phys. Rev. B**52**, 7834 (1995).

[4] R. Jankowiak, R. Richert and H. Bässler, J. Phys. Chem. **89**, 4569 (1985).

[5] Y. Kanematsu, R. Shiraishi, A. Imaoka, S. Saikan and T. Kushida, J. Chem. Phys. **91**, 6579 (1989).

[6] W. Köhler, J. Meiler and J. Friedrich, Phys. Rev. B**35**, 4031 (1987).

[7] T. Kawazoe and Y. Masumoto, Phys. Rev. Lett. **77**, 4942 (1996).

[8] M. Certier, C. Wecker and S. Nikitine, J. Phys. Chem. Solids **30**, 2135 (1969).

[9] S. A. Payne, L. L. Chase and L. A. Boatner, J. Lumin. **35**, 171 (1986).

[10] J. D. Barrie, B. Dunn, G. Hollingsworth and J. I. Zink, J. Phys. Chem. **93**, 3958 (1989).

[11] H. Kishishita, Phys. Status Solidi B**55**, 399 (1973).

[12] S.-H. Wei, S. B. Zhang and A. Zunger, Phys. Rev. Lett. **70**, 1639 (1993).

[13] C. H. Park and D. J. Chadi, Phys. Rev. Lett. **76**, 2314 (1996).

[14] V. Luaña and M. Flórez, J. Chem. Phys. **97**, 6544 (1992): M. Flórez, M. A. Blanco, V. Luaña and L. Pueyo, Phys. Rev. B**49**, 69 (1994).

Figure captions

Fig. 5.1.1. Persistent spectral holes of CuCl nanocrystals embedded in a NaCl crystal at 2 K. The mean radius of the quantum dots is 3.5 nm. Dash-dotted and solid lines in columns (a) represent the absorption spectra before and after the laser exposure, respectively. Dashed and solid lines in columns (b) represent the absorption-spectral change measured at 2 min and 20 min after the burning laser is stopped. The burning photon energy, the energy density, the pulse duration, the pulse repetition and the excitation period are 3.245 eV, 33 μJ/cm^2, 5 ns, 30 Hz and 3 min, respectively. A solid circle represents the main hole. The triangles and square symbols indicate satellite holes.

Fig. 5.1.2. Laser-exposure-time-dependence of spectral holes: (a) absorption spectrum; (b) hole spectra as a function of the exposure time: (A) 10 s, (B) 100 s and (C) 1000 s; (c) hole depth plotted as a function of the exposure time. The circle symbols indicate the experimental results. The dashed lines show the calculated results on the assumption of Gaussian distribution of the burning rates. The standard deviations of the distribution obtained by fitting are σ=3.5. The sample was excited by the 30-Hz dye laser pulses with the energy density of 0.04 μJ/cm^2 and the pump photon energy of 3.245 eV.

Fig. 5.1.3. Spectral holes of thermally annealed CuCl nanocrystals embedded in a NaCl crystal after the intense laser exposure as a function of the cycling temperature: (a) absorption spectra; (b) absorption-spectral change recorded after the elevated temperature: (A) 30, (B) 45 and (C) 75 K. Open circle and triangles represent the main hole and antiholes, respectively; (c) Normalized hole area of CuCl quantum dots as a function of the cycling

temperature T. After hole-burning at T_b and cycling through the elevated temperature T, the hole is measured at T_b again. The dashed lines represent the calculated results on the model described in Ref. 6 and are the fitting by the following expressions; $0.15(1-0.016\sqrt{T})/(1-0.016\sqrt{30})$ [$T > 50$ K] and $0.15(1-0.016\sqrt{T})/(1-0.016\sqrt{30})+0.85(1-0.084\sqrt{T})/(1-0.084\sqrt{30})$ [$T < 50$ K]. The temperature-cycling measurements were done after the samples are excited by 1,800 shots of the laser pulses at the pump photon energies of 3.245 eV with the energy density of 40 μJ/cm^2.

Fig. 5.1.4. Laser-exposure-time-dependence of absorption- and photoluminescence (PL) spectra of CuCl nanocrystals embedded in a NaCl crystal under the 3.492-eV laser excitation with the 30-Hz pulse duration and the 0.85-μJ/cm^2 energy density: (a) absorption spectrum; (b) absorption-change spectra measured after the laser exposure for 300 s (dotted line) and 3000 s (solid line); (c) PL spectra measured after the laser exposure for 0 s (dash-dotted line), 300 s (dotted line) and 3000 s (solid line); (d) Peak energies of absorption spectra (solid circles) vs those of well-exposed absorption-change spectra (crosses) and of well-exposed PL spectra (open circles).

Fig. 5.1.5. Photoluminescence (PL) spectral-change of Cu^+ dimers at T_b=25 K under the 3.492-eV and 30-Hz excitation: (a) PL spectra measured after the 0-s (dash-dotted line), 300-s (dotted line) and 3000-s (solid line) laser exposure with the 8.5-μJ/cm^2 energy density; (b) PL spectra after the temperature cycling at 100 K (dash-dotted line), 150 K (dotted line), 175 K (dashed line) and 200 K (solid line) under the laser irradiation with the 420-nJ/cm^2 energy density. The temperature-cycling measurements were done after the 1-min laser

exposure with the 850-$\mu J/cm^2$ energy density.

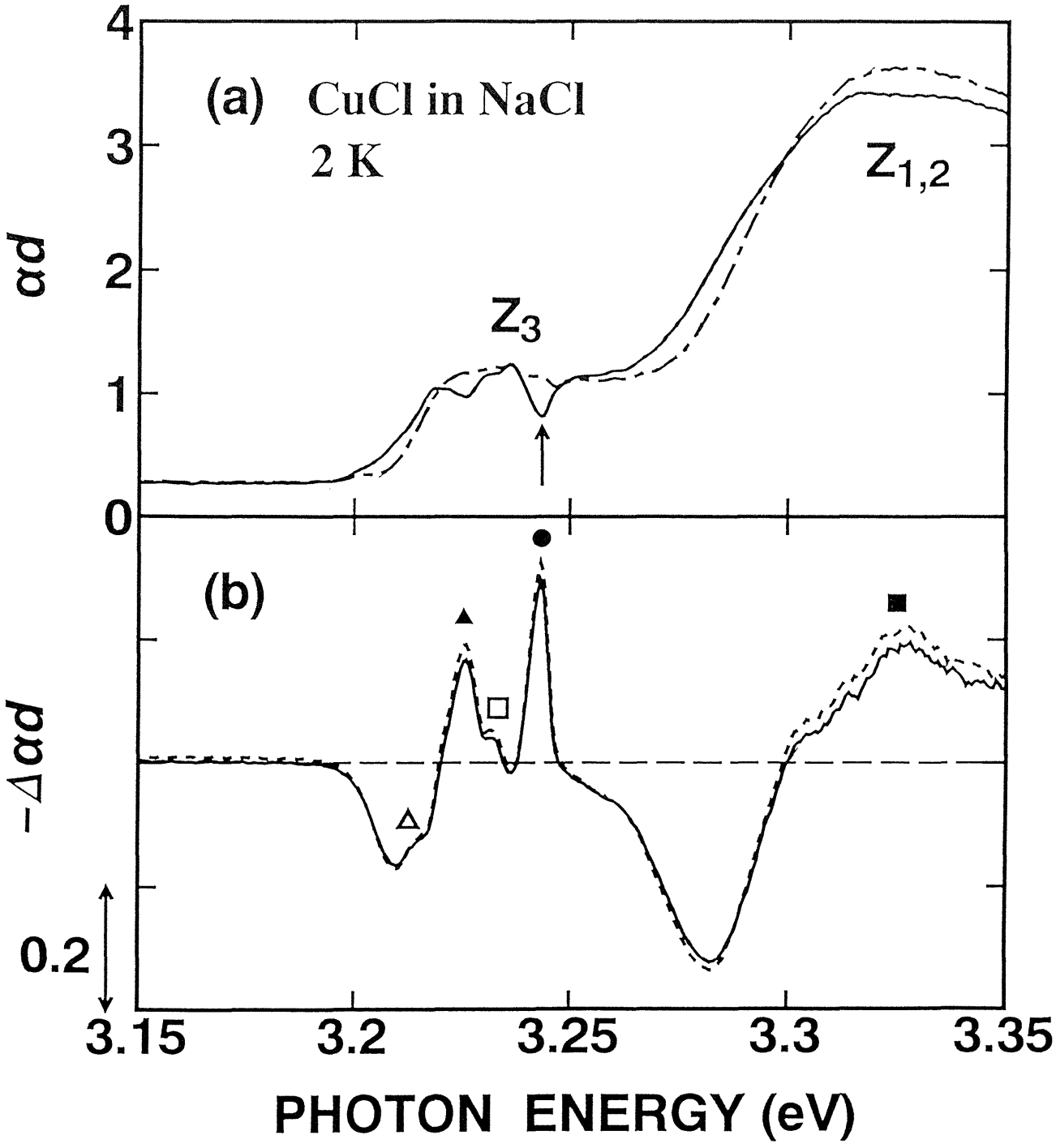
(a) CuCl in NaCl
2 K
$Z_{1,2}$
Z_3
αd
(b)
$-\Delta\alpha d$
0.2
4
3
2
1
0
3.15
3.2
3.25
3.3
3.35
PHOTON ENERGY (eV)

Fig. 5.1.1

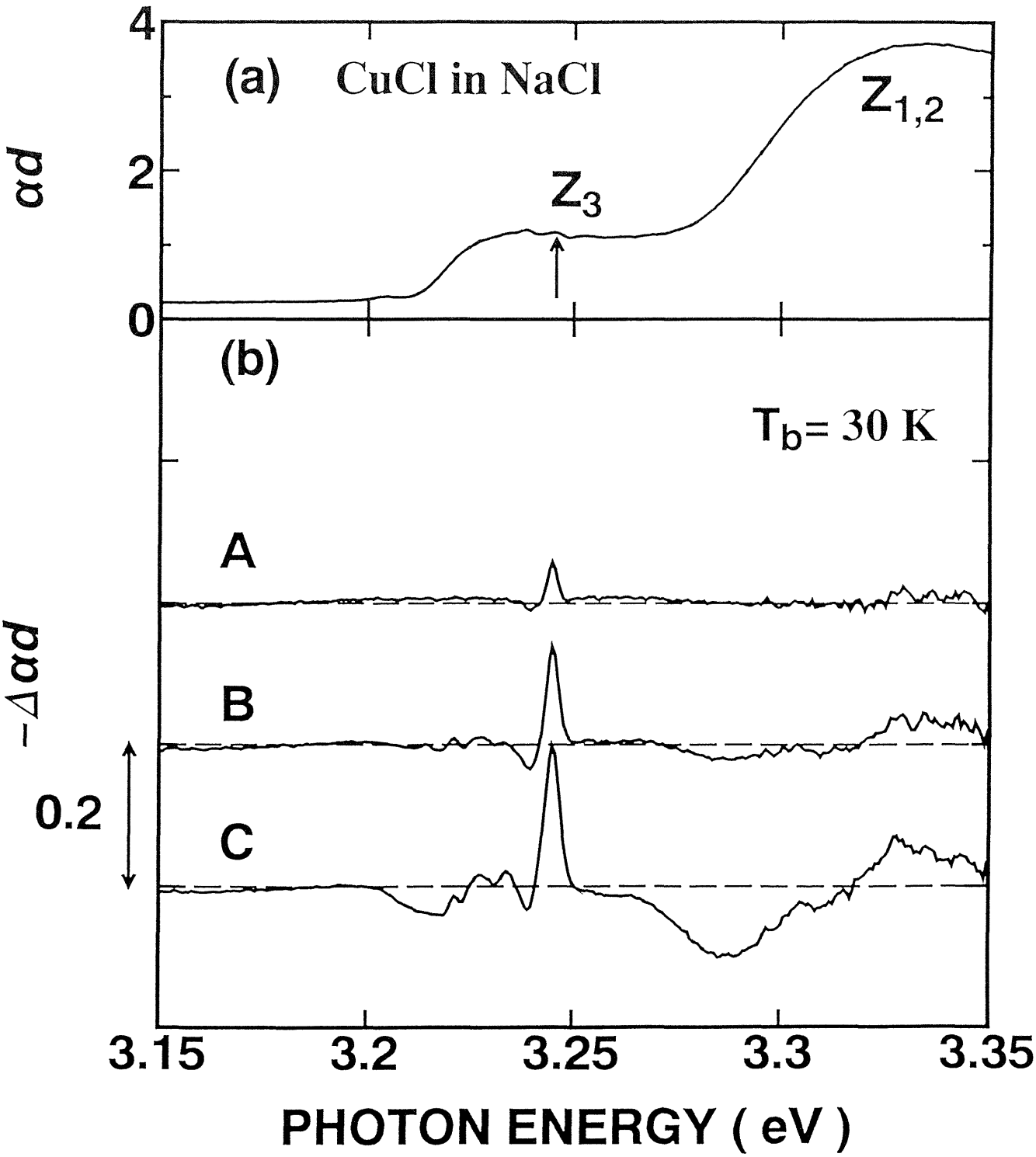
4
2
0
αd
(a) CuCl in NaCl
$Z_{1,2}$
Z_3
(b)
T_b= 30 K
A
B
C
$-\Delta\alpha d$
0.2
3.15
3.2
3.25
3.3
3.35
PHOTON ENERGY (eV)

Fig. 5.1.2

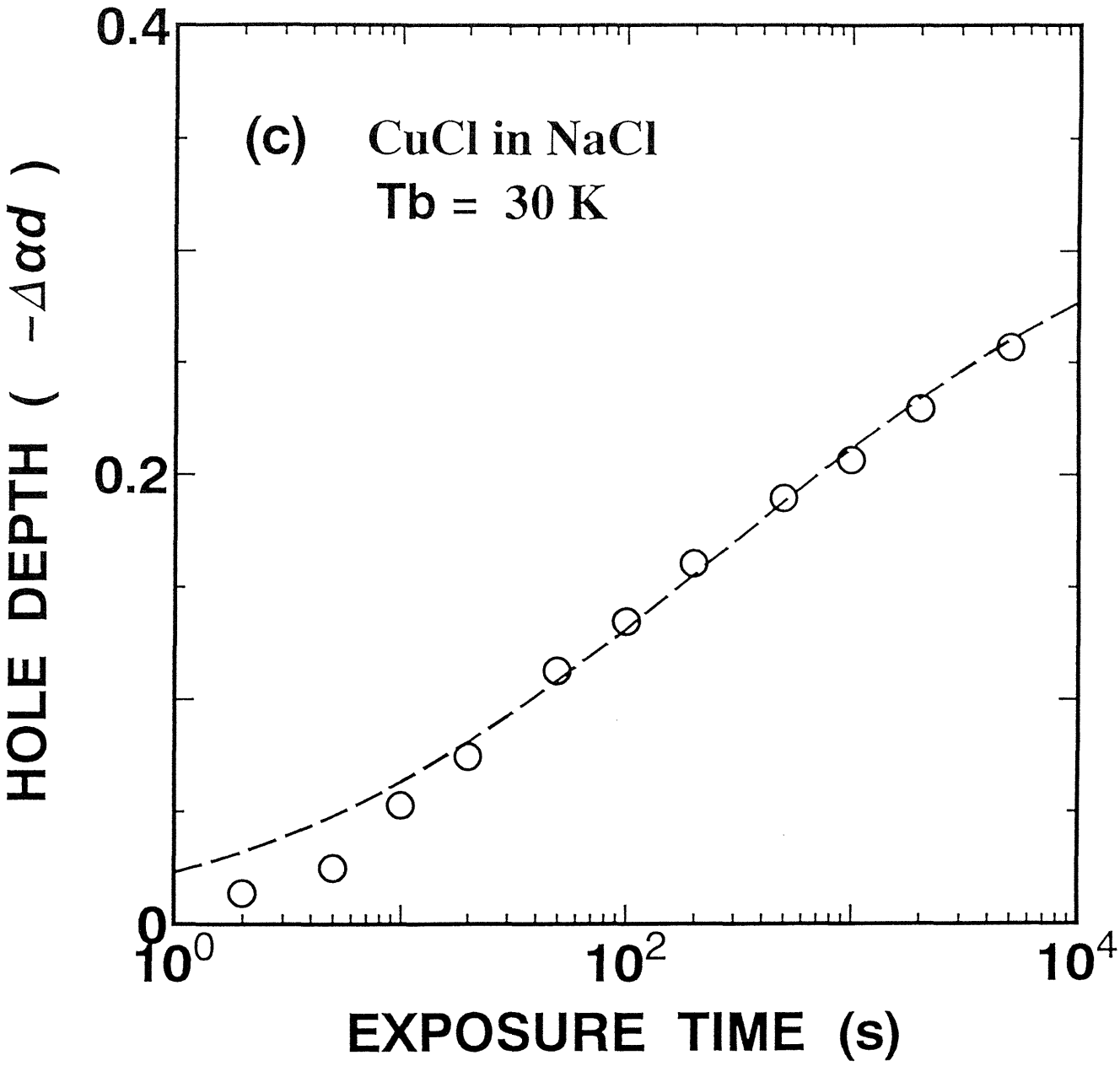
(c) CuCl in NaCl
Tb = 30 K
HOLE DEPTH (−Δαd)
0.4
0.2
0
10^0
10^2
10^4
EXPOSURE TIME (s)

Fig. 5.1.2

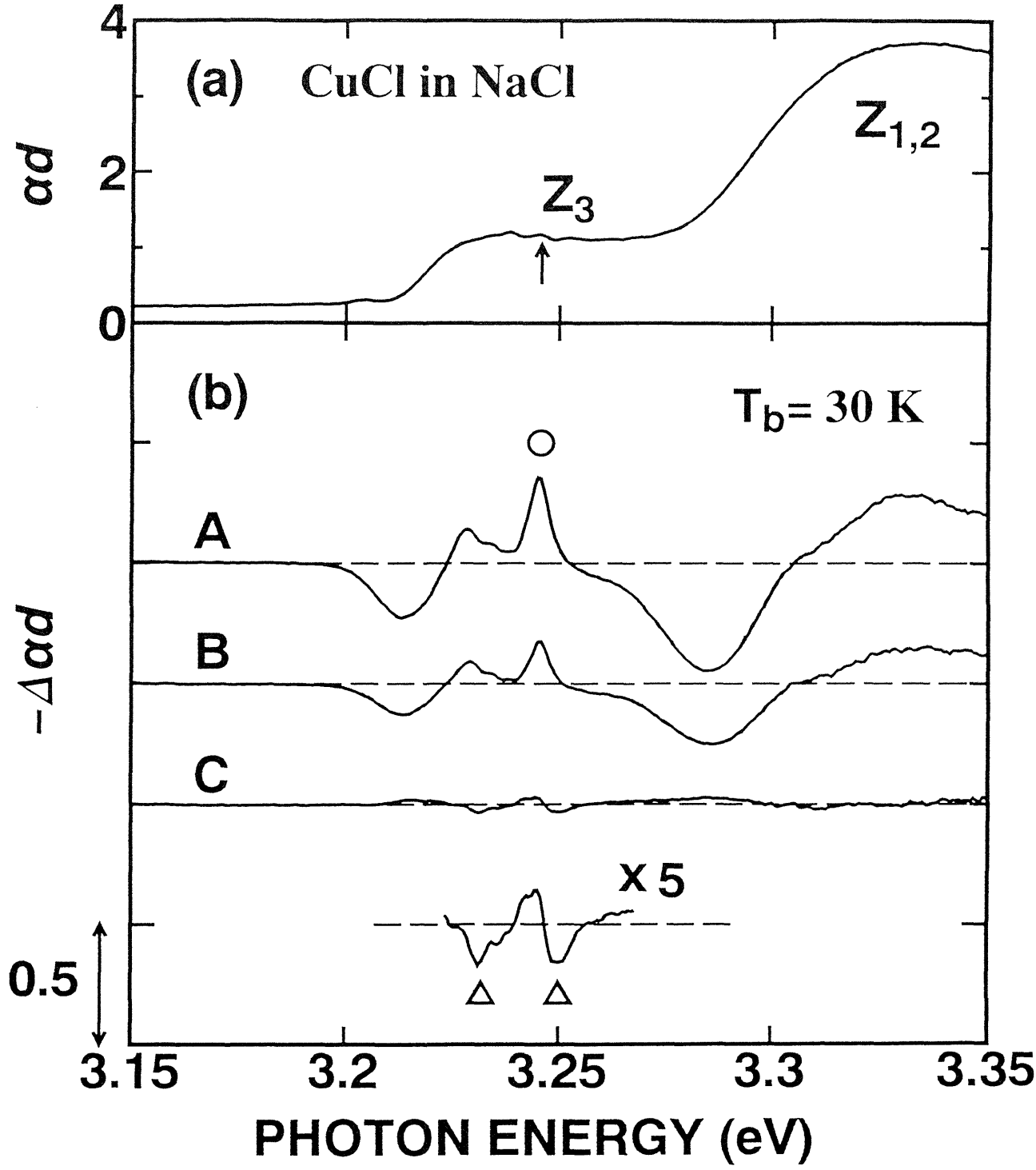
(a) CuCl in NaCl
$Z_{1,2}$
Z_3
αd
4
2
0
(b)
T_b= 30 K
A
B
C
x 5
$-\Delta\alpha d$
0.5
3.15
3.2
3.25
3.3
3.35
PHOTON ENERGY (eV)

Fig. 5.1.3

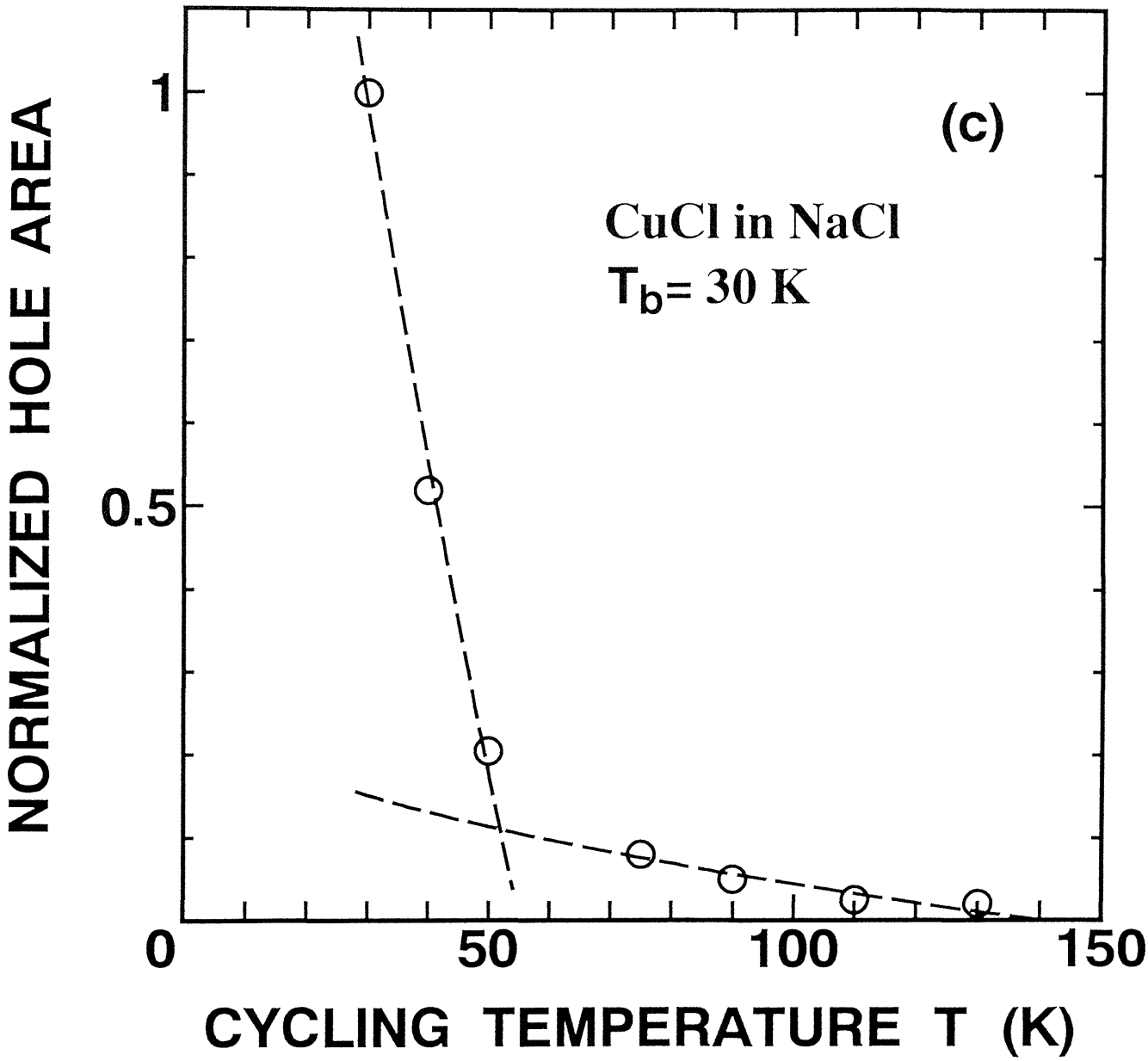
NORMALIZED HOLE AREA
1
0.5
0
50
100
150
CYCLING TEMPERATURE T (K)
(c)
CuCl in NaCl
T_b= 30 K

Fig. 5.1.3

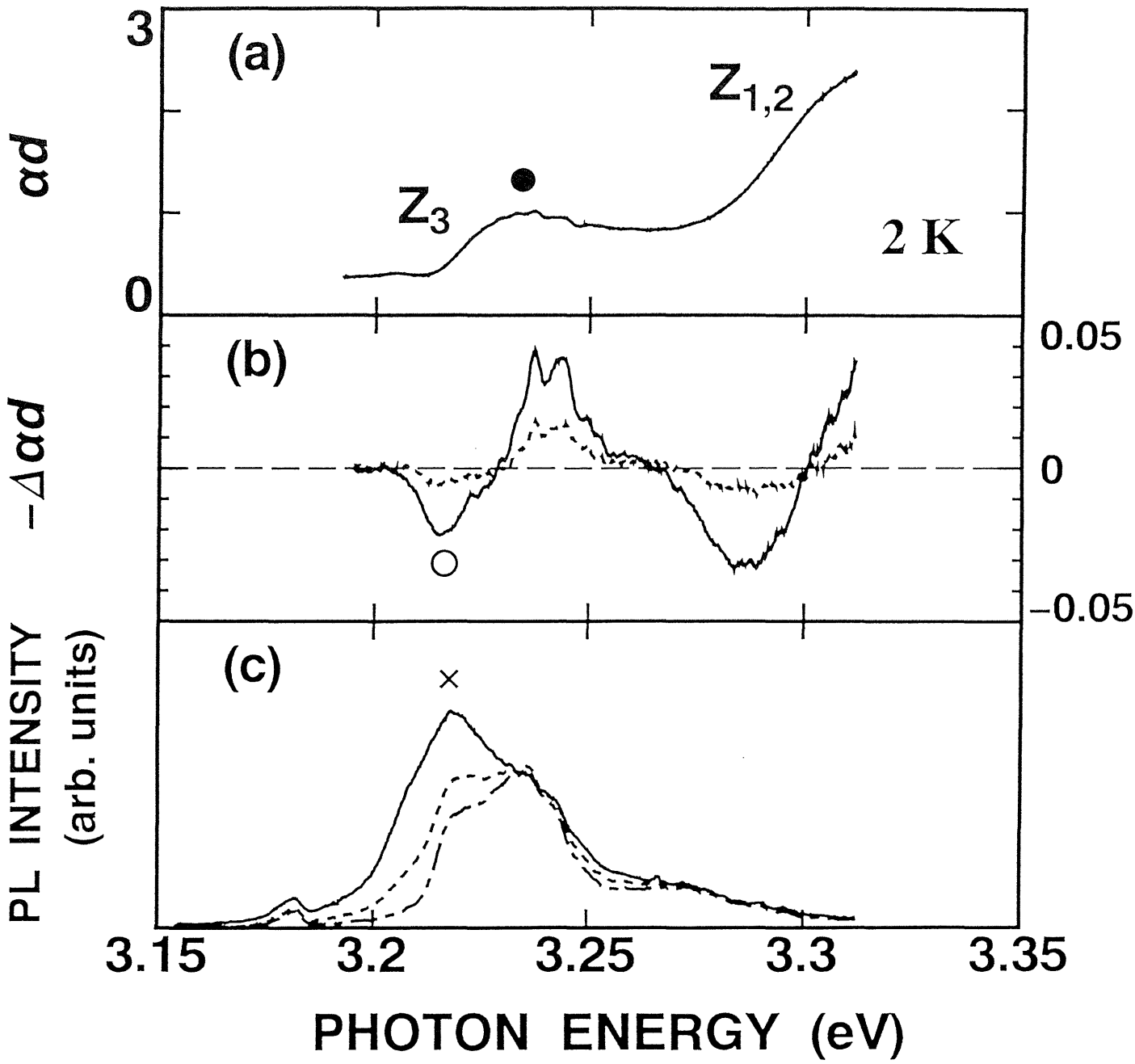
(a)
$Z_{1,2}$
Z_3
2 K
3
0
αd
(b)
0.05
0
−0.05
−Δαd
(c)
PL INTENSITY
(arb. units)
3.15
3.2
3.25
3.3
3.35
PHOTON ENERGY (eV)

Fig. 5.1.4

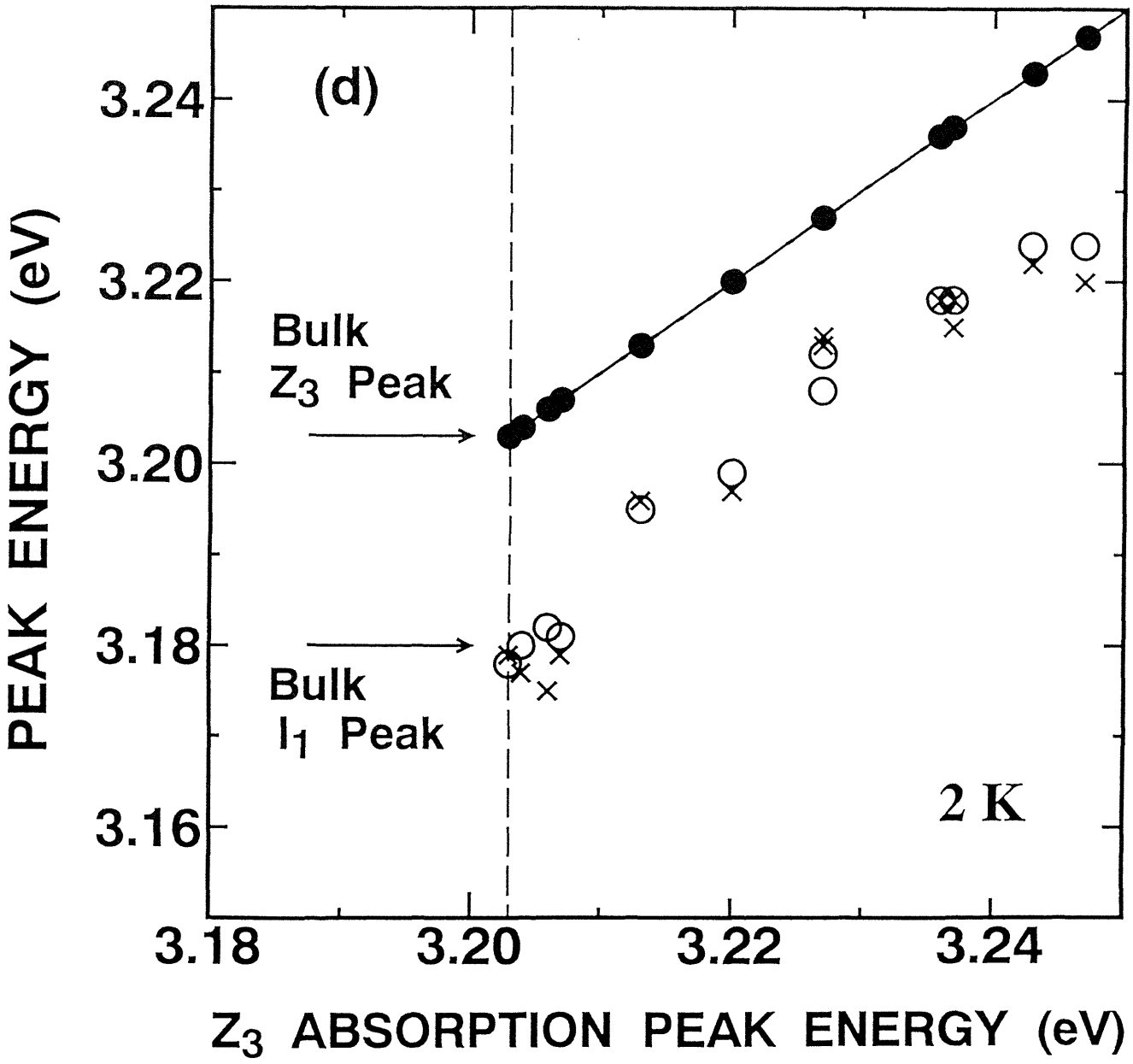
(d)
3.24
3.22
3.20
3.18
3.16
PEAK ENERGY (eV)
Bulk
Z_3 Peak
Bulk
I_1 Peak
2 K
3.18
3.20
3.22
3.24
Z_3 ABSORPTION PEAK ENERGY (eV)

Fig. 5.1.4

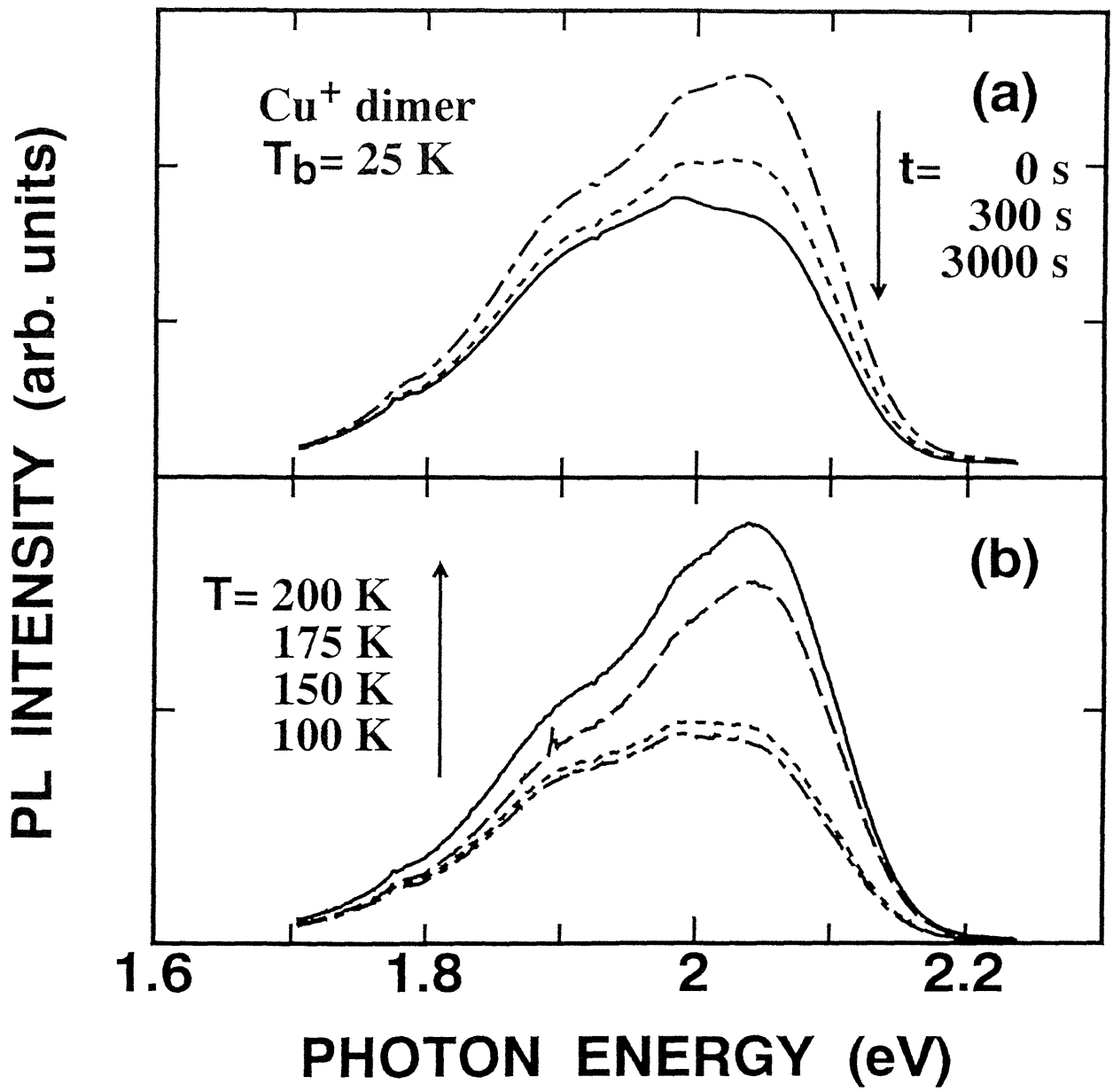
Cu+ dimer
Tb= 25 K
(a)
t= 0 s
300 s
3000 s
(b)
T= 200 K
175 K
150 K
100 K
PL INTENSITY (arb. units)
1.6
1.8
2
2.2
PHOTON ENERGY (eV)

Fig. 5.1.5

5.2 CuCl Nanocrystals Embedded in Aluminoborosilicate Glass

In this section, we investigate the PSHB phenomena of CuCl nanocrystals in aluminoborosilicate glass by means of laser-exposure-time evolution of hole-depth, temperature-cycle experiments, and laser-induced hole-filling experiments. The PSHB phenomena can be explained by the two-level-system (TLS) model. The results imply that there are also two types of TLS's, similar to CuCl nanocrystals embedded in a NaCl crystal. However, the mechanisms of the PSHB phenomena seem to be much different between the glass and the NaCl matrices because the wavy structures coming from the redshift-like absorption changes are not observed in case of glass matrix. We speculate the mechanism of the PSHB phenomena of CuCl nanocrystals embedded in glass.

5.2.1 Demonstration of PSHB Phenomena in CuCl Nanocrystals Embedded in Glass

Figures 5.2.1 (a) show the absorption spectra of CuCl nanocrystals embedded in glass [1] at 2 K. The dash-dotted lines in Fig. 5.2.1 (a) represent the spectra before the dye laser irradiation. Z_3-exciton absorption band in the figure is inhomogeneously broadened, and presents the blue shift from its position in bulk CuCl. The blue-shifts is 37 meV. The mean radius of the nanocrystals estimated from the blue shifts on the exciton quantum confinement model [2,3] is almost consistent with the SAXS results.

The absorption spectra are changed after the laser exposure, as indicated by solid lines in Fig. 5.2.1 (a). The samples are excited by 1,800 laser shots at the pump photon energy of 3.245 eV with the energy density of 33 $\mu J/cm^2$. Figure 5.2.1 (b) displays the absorption-spectral change of the glass. The hole spectra were recorded at 2 min (dotted lines) and at

20 min (solid lines) after the laser exposure was stopped. The features of the hole spectra of the glass sample in Fig. 5.2.1 (b) are summarized as follows: (i) the main spectral-hole denoted by a solid circle and antiholes coming from the induced absorption denoted by open circles are clearly observed; (ii) the main hole area is almost equal to the antiholes area.

5.2.2 Laser-Exposure-Time Evolution Hole-Depth

Figure 5.2.2 shows the laser-exposure-time dependent hole spectra of the glass. The hole depth grows nearly in proportion to the logarithm of the laser exposure time, as shown in Fig. 5.2.2 (c). The spontaneous decay of the hole depth was found to be proportional to the logarithm of time [4]. Fitting the expression given by Ref. 5 for the experimental results, we obtain the standard deviation σ=2.1 for the Gaussian distribution of the burning rate, as mentioned in Sec. 2.2. The experimental hole-depth results are well reproduced by the calculation, as shown in Fig. 5.2.2 (c).

5.2.3 Temperature-Cycling Hole-Filling

The hole structures are erasable by the temperature rise. The absorption spectrum-change of the glass sample after the temperature cycling is displayed in Fig. 5.2.3. This experimental sequence was described in Sec. 5.1.3. Above the cycling temperature of 200 K, the spectral hole as well as the antiholes simultaneously disappear. In case of NaCl matrix, the abrupt spectral-changes are observed at the cycling temperature around 50 K, as mentioned in Sec. 5.1.3. However, in case of the glass matrix, similar spectral-changes are not observed.

Figures 5.2.3 (c) shows the hole area plotted as a function of the cycling temperature. The cycling-temperature-dependent hole area have been fitted by the functional form of $(1-\sqrt{kT\ln(\nu_0 t)/V_{0max}})/(1-\sqrt{kT_b\ln(\nu_0 t)/V_{0max}})$ for $kT\ln(\nu_0 t)<V_{0max}$ [6], as mentioned in Sec. 2.3. The maximum barrier height estimated is 340~370 meV for T<125 K and 560~620 meV for T>125 K. This suggests the coexistence of two kinds of TLS's, similar to CuCl nanocrystals embedded in NaCl crystals.

5.2.4 Laser-Induced Hole-Filling

The hole structures are also erasable by the light exposure. Figure 5.2.4 shows an example of the laser-induced hole-filling. The experimental sequence is as follows: First, several spectral-holes were formed by tuning laser photon energies; next, the laser light with other photon energy (hole-filling laser light) is irradiated. The laser-induced hole-filling occurs more efficiently as the energy intervals between spectral holes and irradiated laser (hole-filling laser light) photon energies are smaller. This suggests that the laser photon energy needed for filling the spectral holes is almost equal to that for creating the spectral holes: The ground-state levels between the double-well potentials in the TLS model is almost same.

5.2.5 Discussions

The area of the antiholes is almost equal to that of the main hole. This observation is an important sign that the PSHB mechanism is photophysical [4,7]. The photophysical process may be attributed to the light-induced structural-change at the nanocrystal-glass

interface and/or the glass itself. This causes many ground-state configuration in both the higher- and the lower-energy side of the main hole, and then the induced absorption at the both sides of the hole [4,7]. In this case, the laser-exposure-time evolution and the temperature-cycling hole-filling rate of the spectral holes are apparently the same with that of antiholes. In fact, the time evolution and the filling rate of the spectral holes and antiholes are same, as shown in Fig. 5.2.2 and 5.2.3. Thus, the photophysical mechanism can well explain the antiholes in both the lower- and the higher-energy side, the temperature-cycling and the laser-induced hole-filling. Therefore, we consider that the PSHB phenomena in CuCl nanocrystals embedded in glass are caused by photophysical mechanisms, such as the photoinduced structural-change at the nanocrystal-glass interface and/or the glass itself.

5.2.6 Summary

In this section, we report on the PSHB phenomena of CuCl nanocrystals embedded in glass. The spectral-hole growth and heat cycle experiments exhibit that the PSHB phenomena can be experiments by the TLS model. There are two kinds of TLS's in the glass sample. The PSHB phenomena is considered to photophysical mechanisms, *e. g.*, photoinduced structural-changes of the nanocrystal and/or the matrix.

References

[1] The composition of the glass sample is as follows; SiO_2: 63.5, B_2O_3: 32.9, Al_2O_3: 1.8, P_2O_5: 0.5, CuCl: 0.5, K_2O: 0.4, Sb_2O_3: 0.4, in a unit of mol%. See, Sec. 4.1.

[2] A. I. Ekimov, Al. L. Efros and A. A. Onushchenko, Solid State Commun. **56**, 921 (1985).

[3] T. Itoh, Y. Iwabuchi and M. Kataoka, Phys. Status Solidi B**145** 567 (1988).

[4] Y. Masumoto, S. Okamoto, T. Yamamoto and T. Kawazoe, Phys. Status Solidi B**188**, 209 (1995).

[5] R. Jankowiak, R. Richert and H. Bässler, J. Phys. Chem. **89**, 4569 (1985).

[6] W. Köhler, J. Meiler and J. Friedrich, Phys. Rev. B**35**, 4031 (1987).

[7] J. K. Gillie, G. J. Small and J. H. Golbeck, J. Phys. Chem. **93**, 1620 (1989) and references therein.

Figure Captions

Fig. 5.2.1. Persistency of spectral holes of CuCl nanocrystals embedded in potassium–aluminoborosilicate glass at 2 K. The dot mean–radius of the glass samples is 2.5 nm. Dash–dotted and solid lines in columns (a) represent the absorption spectra before and after the laser exposure. Dotted and solid lines in columns (b) represent the absorption spectrum change measured 2 min and 20 min after the burning laser is stopped. The burning photon energy, the energy density, the pulse duration, the pulse repetition and the excitation period are 3.245 eV, 33 μJ/cm^2, 5 ns, 30 Hz and 3 min, respectively. The solid and the open circles represent the main holes and the antiholes, respectively.

Fig. 5.2.2. Spectral–hole growth of CuCl nanocrystals embedded in glass as a function of the laser exposure time: (a) the absorption spectra; (b) the absorption–spectral change after the laser exposure for 1 s (A), 10 s (B), 100 s (C) and 1000 s (D). The burning photon energy, the energy density, the pulse duration, the pulse repetition are 3.253 eV, 0.04 μJ/cm^2, 5 ns, 30 Hz, respectively; (c) hole depth of CuCl nanocrystals in glass as a function of the burning time. The circle symbols indicate the experimental results. The dashed lines show the calculated results on the assumption of Gaussian distribution of the burning rates. The standard deviations of the distribution obtained by the fitting are σ=2.1.

Fig. 5.2.3. Spectral–hole thermal–annealing of CuCl nanocrystals embedded in glass as a function of the cycling temperature: (a) the absorption spectra; (b) the absorption–spectral change recorded after the sample temperature is elevated at 15 K (A), 50 K (B), 100 K (C)

and 150 K (D). The burning photon energy, the energy density, the pulse duration, the pulse repetition and the excitation period are 3.253 eV, 40 μJ/cm^2, 5 ns, 30 Hz and 1 min, respectively; (c) normalized hole area of CuCl nanocrystals in glass plotted as a function of cycling temperature. After hole-burning at T_b and cycling through the elevated temperature T, the hole is measured at T_b again. The dashed lines represent the calculated results on the model described in Ref. 6. The samples are excited by 1,800 shots of the laser pulses at the pump photon energies of 3.253 eV with the energy density of 40 μJ/cm^2. The dashed lines are the fitting by the following expressions; $0.25(1-0.073\sqrt{T})/(1-0.073\sqrt{15})$ [T>125 K] and $0.25(1-0.073\sqrt{T})/(1-0.073\sqrt{15})+0.75(1-0.090\sqrt{T})/(1-0.090\sqrt{15})$ [T < 125 K].

Fig. 5.2.4. An example of the laser-induced hole-filling of CuCl nanocrystals embedded in glass. The experimental sequence is as follows: Firstly, five spectral holes are formed as denoted by the dotted line in the figure. The hole energies are 3.280, 3.271, 3.263, 3.254, 3.246 and 3.237 eV. Finally, the sample is exposed under the 3.250-eV laser excitation.

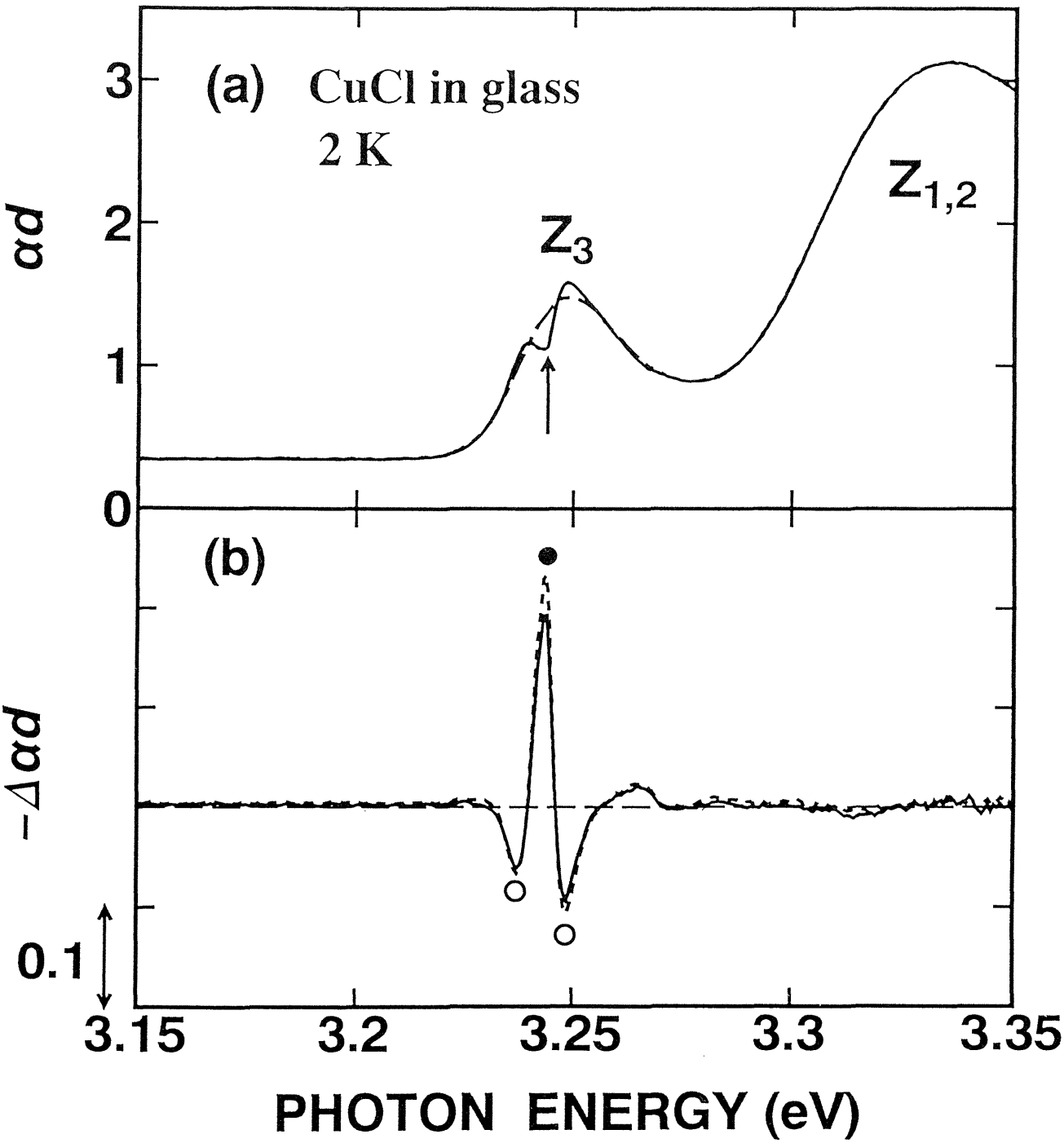
(a) CuCl in glass
2 K
Z_3
$Z_{1,2}$
αd
(b)
$-\Delta\alpha d$
0.1
3
2
1
0
3.15
3.2
3.25
3.3
3.35
PHOTON ENERGY (eV)

Fig. 5.2.1

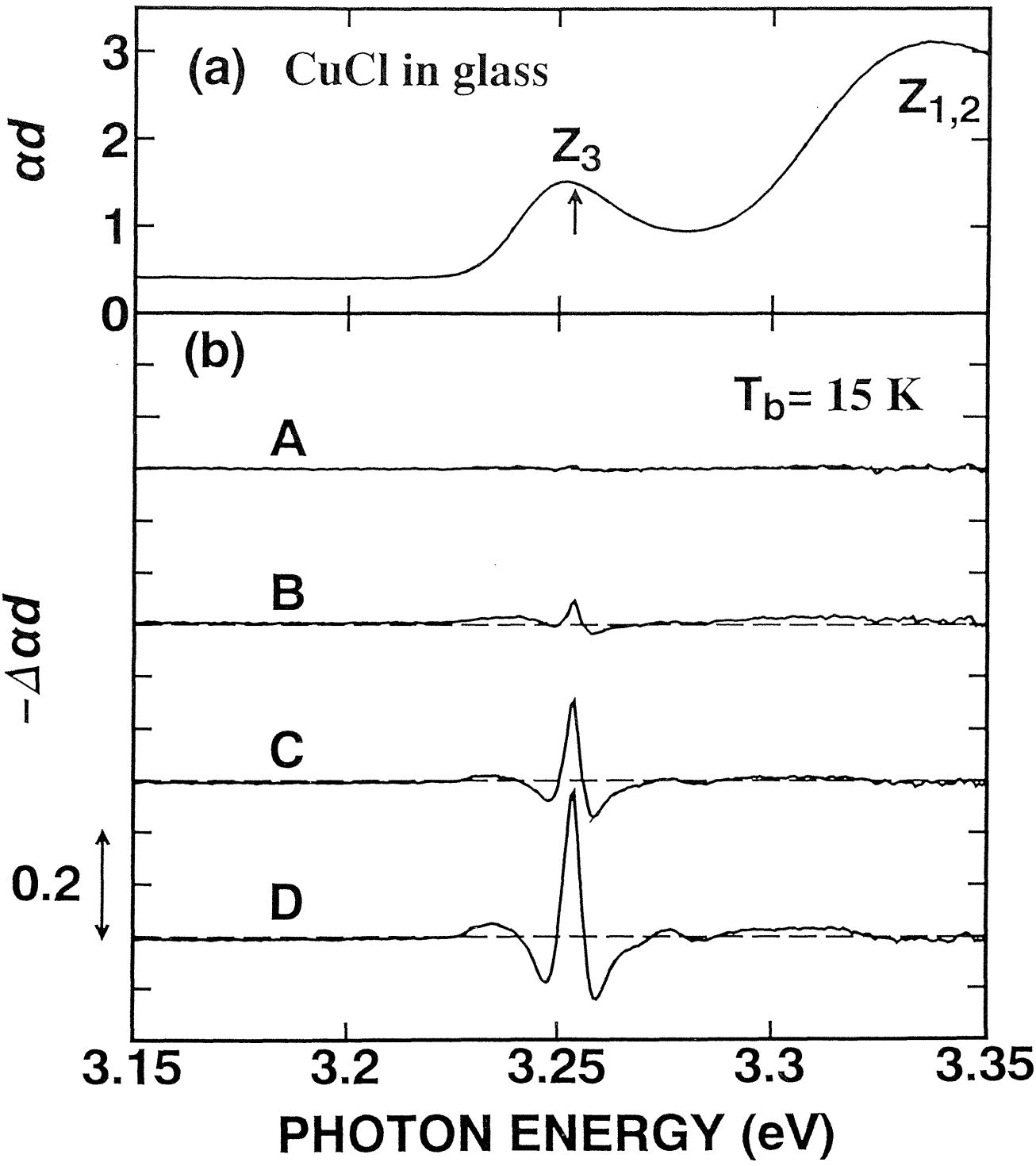
(a) CuCl in glass
$Z_{1,2}$
Z_3
αd
3
2
1
0
(b)
T_b= 15 K
A
B
C
D
$-\Delta\alpha d$
0.2
3.15
3.2
3.25
3.3
3.35
PHOTON ENERGY (eV)

Fig. 5.2.2

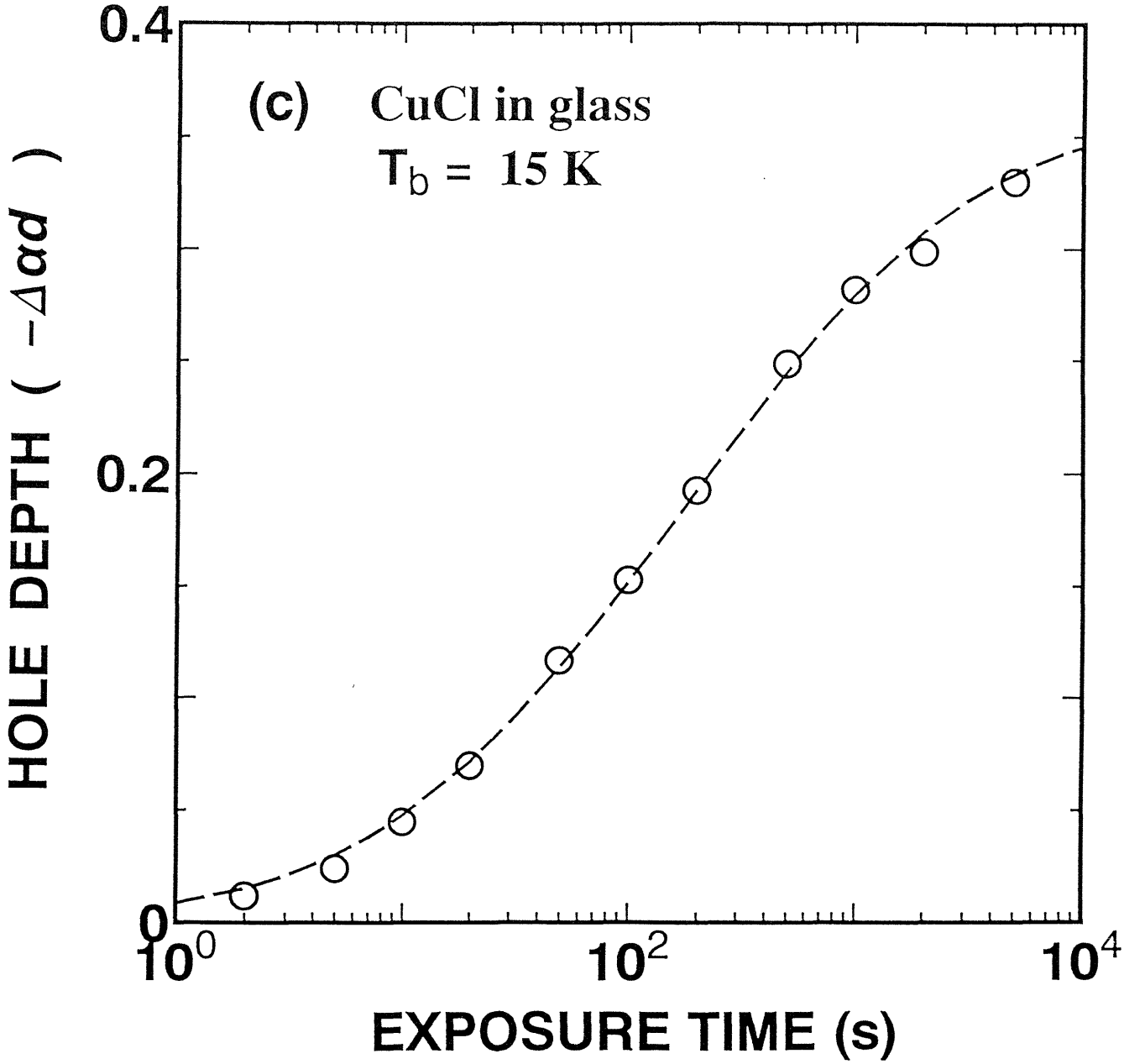
(c) CuCl in glass
T_b = 15 K
HOLE DEPTH ($-\Delta\alpha d$)
0.4
0.2
0
10^0
10^2
10^4
EXPOSURE TIME (s)

Fig. 5.2.2

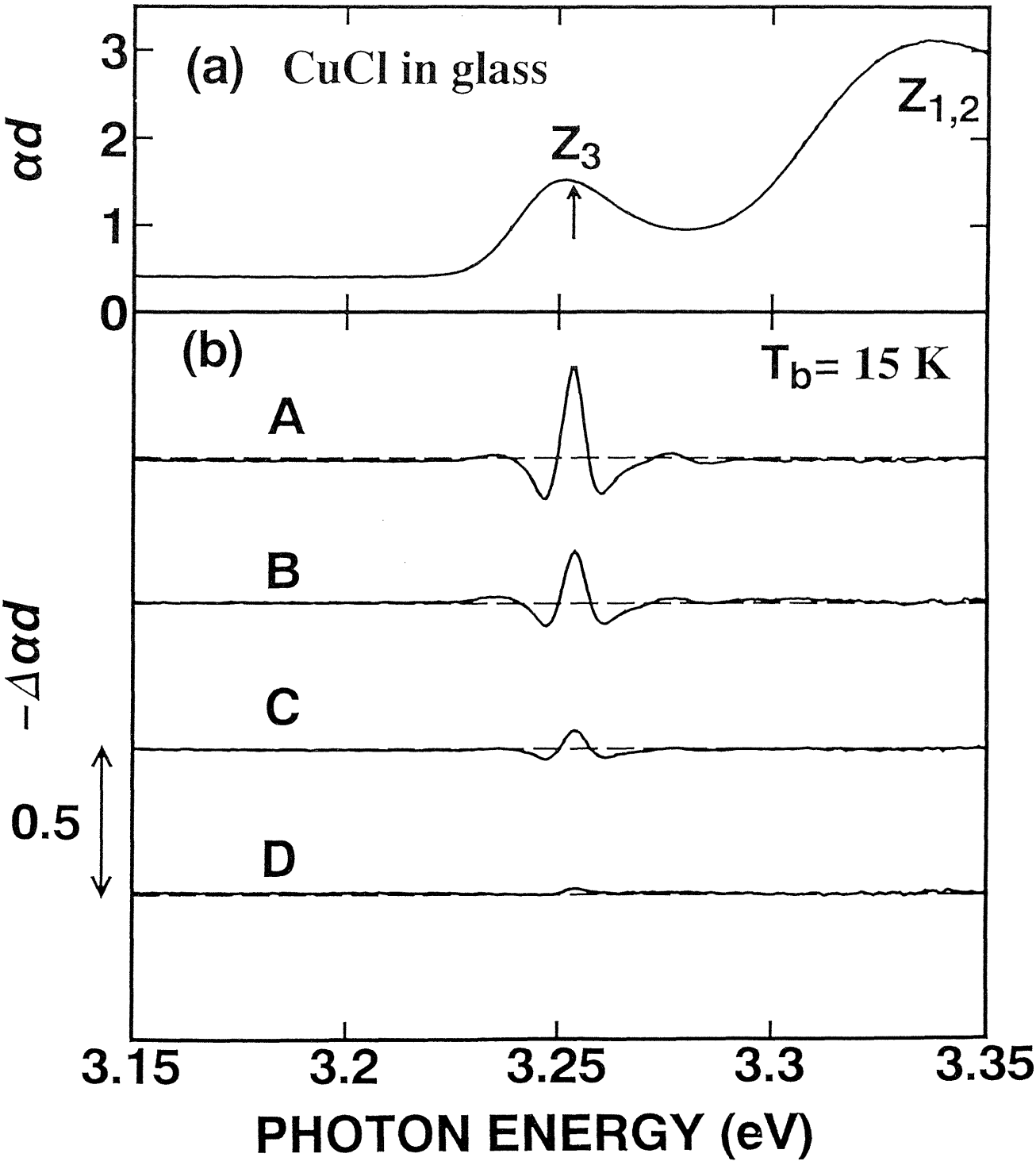
(a) CuCl in glass
$Z_{1,2}$
Z_3
αd
3
2
1
0
(b)
T_b= 15 K
A
B
C
D
$-\Delta\alpha d$
0.5
3.15
3.2
3.25
3.3
3.35
PHOTON ENERGY (eV)

Fig. 5.2.3

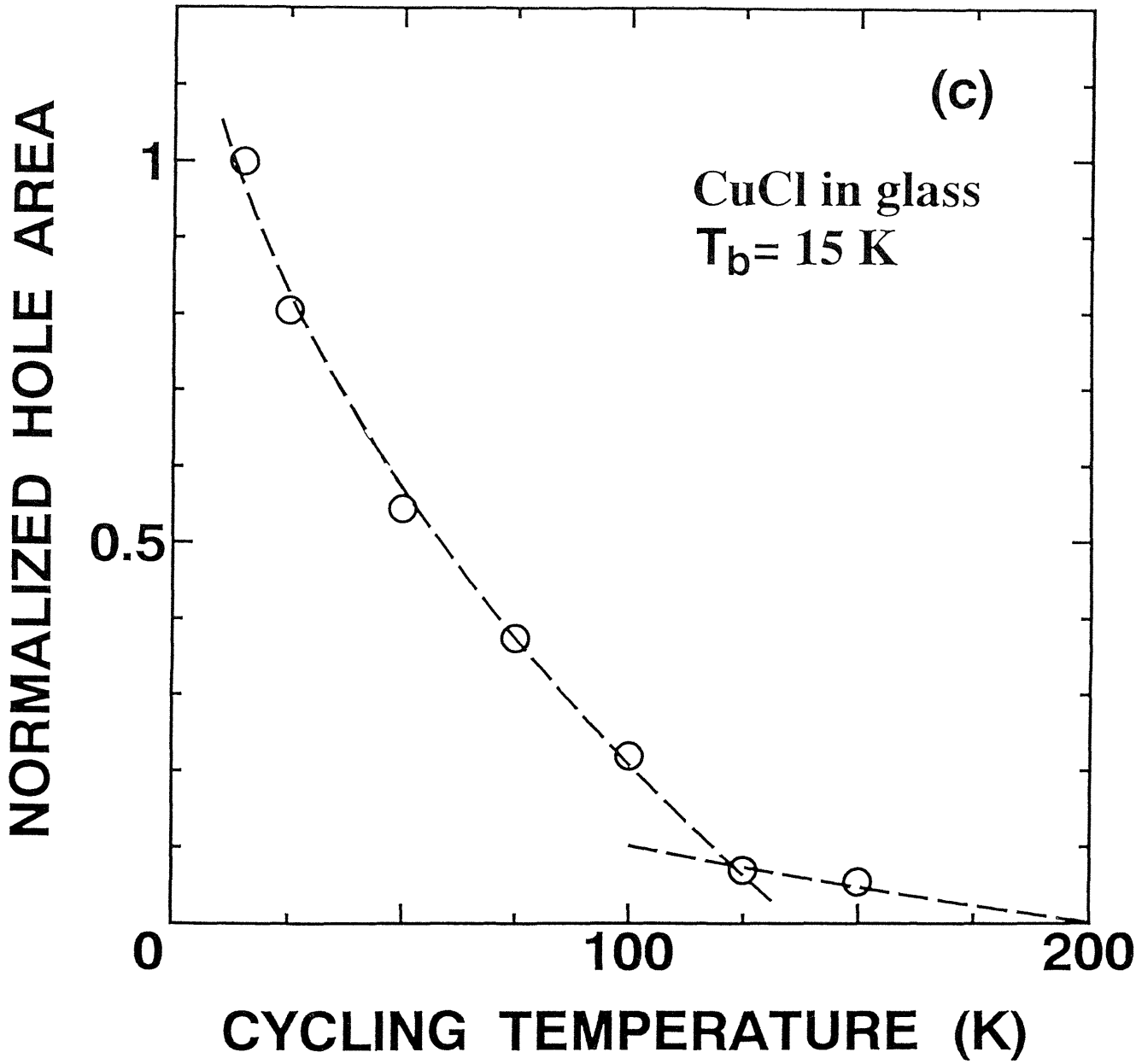
(c)
CuCl in glass
T_b= 15 K
NORMALIZED HOLE AREA
1
0.5
0
100
200
CYCLING TEMPERATURE (K)

Fig. 5.2.3

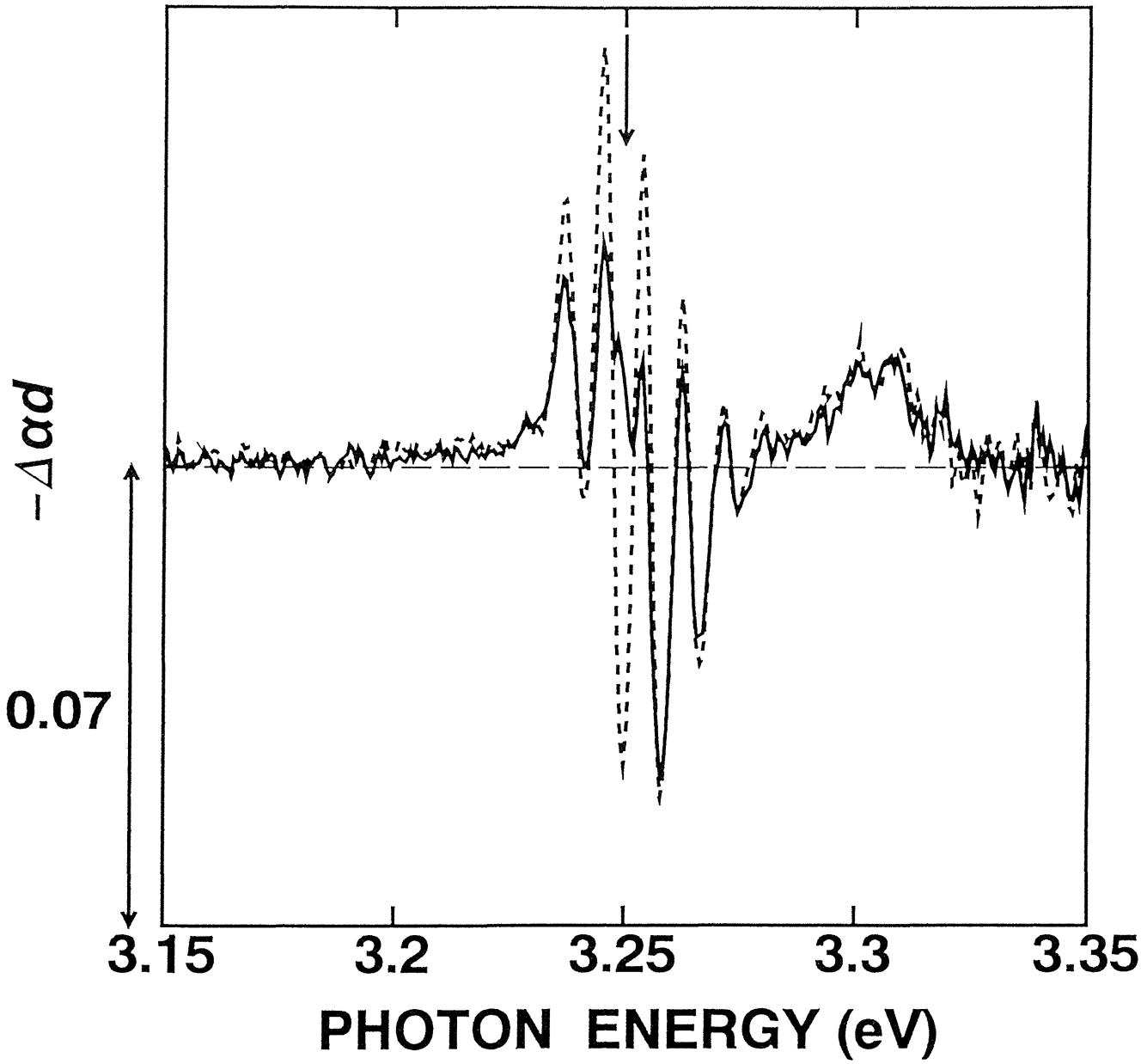

Fig. 5.2.4

Chapter VI

Applications of Persistent Spectral Hole-Burning (PSHB) Phenomena in CuCl Nanocrystals

In this chapter, we discuss possible applications of persistent spectral hole-burning (PSHB) phenomena in CuCl nanocrystals: Site-selective spectroscopies and optical memories. In particular, we exhibit some examples of the applications: In Sec. 6.1, we have measured size-dependent acoustic phonons confined in CuCl nanocrystals and have discussed the matrix-dependence of the phonon energies; in Sec. 6.2, we have shown the size-dependent higher excited states of excitons confined in CuCl nanocrystals. The energies were almost consistent with the calculated results on the exciton confinement; in Sec. 6.3, we have demonstrated frequency-domain optical data storage. We succeeded in sequential hole formation in the Z_3-exciton absorption band of CuCl nanocrystals. This implies that CuCl nanocrystal may be used as an optical memory.

6.1 Observation of Acoustic Phonons Confined in CuCl Nanocrystals

Unique optical properties of the nanocrystals are caused by the three-dimensional confinement of phonons as well as electrons, holes and excitons in small volumes. The interaction between the confined carriers and phonons is an important factor that determines the optical properties.

So far, Raman spectroscopy is the most popular method to investigate the acoustic phonons confined in nanocrystals. Duval *et al.* reported the appearance of a low-frequency

Raman peak for glass containing nanocrystals which were as small as 10 nm [1]. They compared the Raman shift with the theoretical eigenfrequencies of elastic vibrational modes of a sphere [2], and concluded that the observed low-frequency Raman peak was due to an acoustic phonon mode confined in the nanocrystals. Similar low-frequency Raman peaks have been studied for a variety of nanocrystals [3-5]. However, by Raman spectroscopy, we can observe confined acoustic phonon modes of the ensemble of the size-dispersed nanocrystals as a whole, but can not obtain the acoustic phonon modes of certain-size nanocrystals.

Instead of Raman spectroscopy, we adopt a persistent hole-burning method. In case of semiconductor nanocrystal systems, the quantum confinement energy depends on the size of nanocrystals, so that we can excite selectively certain-size nanocrystals by tuning the pump photon energy, as was mentioned in Sec. 3.2. Thus, we can observe the hole spectra of nanocrystals of a certain-size. In this section, we describe the size-dependent confined acoustic phonons in CuCl nanocrystals.

The Z_3-exciton absorption band of CuCl nanocrystals is inhomogeneously broadened owing to the size distribution. After the narrow-band laser irradiation in the Z_3-exciton absorption band, the zero-phonon line and its phonon sidebands are clearly observed. The energy intervals between the zero-phonon line and its phonon sidebands are inversely proportional to the diameter of nanocrystals which are excited selectively with the simultaneous emission of phonons. The intervals are in good agreement with the calculated energies of the confined acoustic phonon modes in an elastic sphere. We conclude that the phonon sidebands appear owing to the emission of confined acoustic phonons in CuCl

nanocrystals. This method is superior to Raman spectroscopy, because it is available for the determination of acoustic phonon modes as a function of the size.

6.1.1 Experimental Results

Figure 6.1.1 shows the linear absorption spectrum (a) and the differential absorption spectra (b) of CuCl nanocrystals embedded in glass at 2 K. The mean radius of the nanocrystals is 2.5 nm. The energy density and the pulse repetition rate are 1.45 mJ/cm^2 and 30 Hz, respectively. The spectra A and B represent the hole spectra at the pump photon energies of 3.2618 and 3.2448 eV, respectively. The energy intervals between the zero-phonon lines and its phonon sidebands decrease with the decrease of the pump photon energy: the energy intervals decrease with the increase of the diameter of nanocrystals. The Debye-Waller factor is found to be much larger than 0.5. Moreover, the phonon sideband peak in the hole-burning spectrum under the weak-limit excitation is much smaller than the zero-phonon peak and the energy position of the phonon sideband peak agrees with that shown in Fig. 6.1.1. With the increase of the pump intensity, the phonon sideband grows, while the zero-phonon line saturates.

Figure 6.1.2 shows the absorption spectrum (a) and the hole spectra (b) of CuCl nanocrystals embedded in glass at 2 K. The mean radius of the nanocrystals is 2.5 nm. The sample is excited by 9,000 laser shots at the pump photon energy of 3.2363 eV with the energy density of 90 μJ/cm^2. The hole spectra as indicated by solid and dotted lines are recorded at 1 min and 30 min after the laser exposure is stopped, respectively. We use a halogen lamp instead of the ASE probe beam in order to prove the persistency of the spectral

holes, as illustrated in Sec. 4.2. In case of glass matrix samples, the zero-phonon line, phonon sidebands and antiholes are clearly observed and are preserved for more than 30 min. These spectra resemble the hole spectra obtained by using the nanosecond pump-and-probe method. The hole spectra in the pump-and-probe experiments consist of both the transient component and the persistent component. In case of glass, more than 70 % of the holes observed by the pump-and-probe method still remains even when the time delay between pump and probe beams is 1.4 s at 2 K [6]. The time 1.4 s is much longer than the laser repetition period. Therefore, the persistent component dominates the hole spectra measured by the pump-and-probe experiments.

Figure 6.1.3 shows the linear absorption spectrum (a) and the differential absorption spectra (b) of CuCl nanocrystals embedded in a NaCl host crystal at 2 K. The mean radius of the nanocrystals is 4.0 nm. The hole spectrum A is obtained by using a tungsten lamp. On the other hand, the spectra B and C are obtained by using a nanosecond pump-and-probe method. The pump photon energy in spectra A and B is 3.2178 eV. Compared with the hole spectrum A, the phonon sidebands and the zero-phonon line are clearly observed in the hole spectrum B, because wavy structures, as indicated by the solid circle in Fig. 6.1.3, are erased. The spectral holes are superposed on the wavy structures coming from the red shift of the absorption spectrum. Since phonon sidebands are superposed on the fairly large wavy structures, we can hardly separate the phonon sidebands. Instead, we can obtain the clear hole spectra without the wavy structures by the nanosecond pump-and-probe method as described in Sec. 4.2. We do not know the reason exactly, but we think that the wavy components are erased owing to the intense probe beam in case of the pump-and-probe method. On the other

hand, the spectral holes are reduced but still remain sufficiently, probably because the filling rate for the wavy structures is higher than that for the holes. Thus, we obtain the hole spectra where the zero-phonon line and its phonon sidebands are clearly observed, but the wavy structures are not. It is noted that the energy intervals between the zero-phonon line and the phonon sidebands also decrease with the decrease of the pump energy in case of NaCl matrix samples.

Figure 6.1.4 shows the relation between the energy intervals and the inverse of the diameter of nanocrystals in both cases of NaCl matrix and glass matrix. The diameter of nanocrystals is calculated from the photon energies of the phonon sidebands, by using Eq. 3.1 in Sec. 3.2. The energy intervals are apparently proportional to the inverse of the diameter of nanocrystals.

6.1.2 Discussions

We clarify that the phonon sideband structures are due to acoustic phonon modes confined in CuCl nanocrystals as follows. The free vibrational modes of an isotropic elastic sphere are investigated theoretically by Lamb [2]. In other words, Lamb had dealt with the confined acoustic phonons in a small sphere. Further extension of the Lamb's theory has been done in Refs. 7 and 8. On these theories, two types of vibrational modes exist in an elastic sphere. They are called spherical modes and torsional modes, and are expressed by the spherical Bessel function. The spherical modes and the torsional modes are characterized by a branch number n and an angular momentum l.

The frequencies of the different modes of a spherical particle are proportional to the

inverse of the diameter. The frequency of the spherical mode of a free particle corresponding to n=1 and l=0 is

$$\omega^1_{0_S} = \frac{5.7}{D} v_l \quad (n = 1, l = 0) \quad , \tag{6.1.1}$$

where D and v_l are the diameter of nanocrystals and the longitudinal sound velocity of the CuCl bulk crystal, respectively. We estimate the longitudinal sound velocity from the elastic constants and the mass density at 4.2 K. The calculated energy of this mode is indicated by the line A in Fig. 6.1.4. This mode is the so-called breathing mode which is illustrated in Fig. 6.1.5 (a).

The frequencies of the lowest-energy spherical and torsional modes specified by n=0 and l=2 are practically equal to:

$$\omega^2_{0_S} = \omega^2_{0_T} = \frac{2.36}{D} v_l \quad (n = 0, l = 2) \quad . \tag{6.1.2}$$

The lowest-energy torsional mode and spherical mode are shown in Fig. 6.1.5 (b) and (c), respectively. This spherical mode is the so-called ellipsoidal mode. The calculated energy of these modes is indicated by the line B in Fig. 6.1.4.

The lowest energy modes with n=0 in the spherical mode correspond to the surface modes and have large amplitudes near the surface of the nanocrystals. On the other hand, the higher energy modes of $n \geq 1$ correspond to the inner modes [7]. Comparing the experimental results with the calculated results, we know that the inner modes of n=1 and l=0 appear in CuCl nanocrystals embedded in a NaCl host crystal. On the other hand, the surface modes of n=0 and l=2 are observed in CuCl nanocrystals embedded in glass. In many kinds of

nanocrystals embedded in glass matrix, the contact between the nanocrystals and the glass matrix is considered not to be very close, so that the surface modes are usually observed [1,3–5]. On the other hand, in case of CuCl nanocrystals embedded in NaCl matrix, the surface of nanocrystals is considered to bond to NaCl matrix, so that the surface modes disappear. This consideration is in agreement with theoretical results, so called "clamping effect" [7].

Slight deviation between the experimental and theoretical results are observed. This deviation is probably due to the shape of the nanocrystals. The shape of the nanocrystals embedded in NaCl crystals is sometimes speculated to be cubic or platelet [9,10].

6.1.3 Summary

We investigated confined acoustic phonons in CuCl nanocrystals by means of a site-selective nanosecond pump–and–probe method. Phonon sidebands appear around the zero-phonon line in the differential absorption spectra at 2 K. The energy intervals between the zero–phonon line and the phonon sidebands are inversely proportional to the diameter of nanocrystals, and coincide with the theoretically calculated energies of vibrational modes of CuCl nanocrystals. We conclude that the phonon sidebands are due to confined acoustic phonons in CuCl nanocrystals.

References

[1] E. Duval, A. Boukenter and B. Champagnon, Phys. Rev. Lett. **56**, 2052 (1986).

[2] H. Lamb, Proc. London Math. Soc. **13**, 187 (1882).

[3] N. N. Ovsyuk, E. B. Gorokhov, V. V. Grishchenko and A. P. Shebanin, JETP Lett. **47**,

298 (1988).

[4] M. Fujii, T. Nagareda, S. Hayashi and K. Yamamoto, Phys. Rev. B **44**, 6243 (1991).

[5] A. Tanaka, S. Onari and T. Arai, Phys. Rev. B **47**, 1237 (1993).

[6] Naoe, L. G. Zimin and Y. Masumoto, Phys. Rev. B **50**, 18200 (1994).

[7] A. Tamura, K. Higeta and T. Ichinokawa, J. Phys. C: Solid State Phys. **15**, 4975 (1982).

[8] N. Nishiguchi and T. Sakuma, Solid State Commun. **38**, 1073 (1981).

[9] T. Itoh, S. Yano, N. Katagiri, Y. Iwabuchi, C. Gourdon and A. I. Ekimov, J. Lumin. **60&61**, 396 (1994).

[10] T. Itoh, Y. Iwabuchi and T. Kirihara, Phys. Status Solidi B**146**, 531 (1988).

Figure Captions

Fig. 6.1.1. Linear absorption spectrum (a) and differential absorption spectra (b) of CuCl nanocrystals in glass at 2 K. The mean radius of the nanocrystals is 2.5 nm. The energy density is 1.45 mJ/cm^2 and the pulse repetition rate is 30 Hz. The spectra A and B represent the hole spectra taken by using a nanosecond pump–and–probe method, with the pump photon energies of 3.2618 and 3.2448 eV, respectively.

Fig. 6.1.2. Absorption spectra (a) and hole spectra (b) of CuCl nanocrystals embedded in glass at 2 K. The mean radius of the nanocrystals is 2.5 nm. The pump energy is 3.2363 eV and the energy density is 90 $\mu J/cm^2$. The pulse repetition rate is 30 Hz and the irradiation time is 5 min. The hole spectra are obtained by using a tungsten lamp. The solid line and the dash–dotted line in (a) represent the absorption spectra before and after the laser irradiation, respectively. The hole spectra in (b) are recorded at 1 min and 30 min after the laser irradiation is stopped, as indicated by solid and dotted lines, respectively.

Fig. 6.1.3. Linear absorption spectrum (a) and differential absorption spectra (b) of CuCl nanocrystals in a NaCl host crystal at 2 K. The mean radius of the nanocrystals is 4.0 nm. The spectrum A represents the hole spectrum recorded by using a tungsten lamp at 2 min after the laser exposure is stopped. The solid circle in the spectrum A indicates the wavy structure discussed in the text. The pump photon energy is 3.2178 eV and the energy density is 180 $\mu J/cm^2$. The pulse repetition rate is 30 Hz and the exposure time is 10 s. The spectra B and C represent the hole spectra by using a nanosecond pump–and–probe method, with the pump

photon energies of 3.2178 and 3.2145 eV, respectively. The energy density and the pulse repetition rate are 1.45 mJ/cm^2 and 30 Hz, respectively.

Fig. 6.1.4. The relation between the crystallite size and the energy of acoustic phonons confined in CuCl nanocrystals at 2 K. Open and solid circles represent the peak energies of the phonon sidebands, in case of NaCl matrix and glass matrix, respectively. Solid lines are the calculated energies of vibrational modes on the elastic sphere model. The solid line A corresponds to the vibrational mode of the breathing mode. The solid line B corresponds to the torsional mode or the ellipsoidal mode.

Fig. 6.1.5. Vibrational eigenmodes of a spherical particle: (a) the breathing mode, (b) the torsional mode, and (c) the ellipsoidal mode.

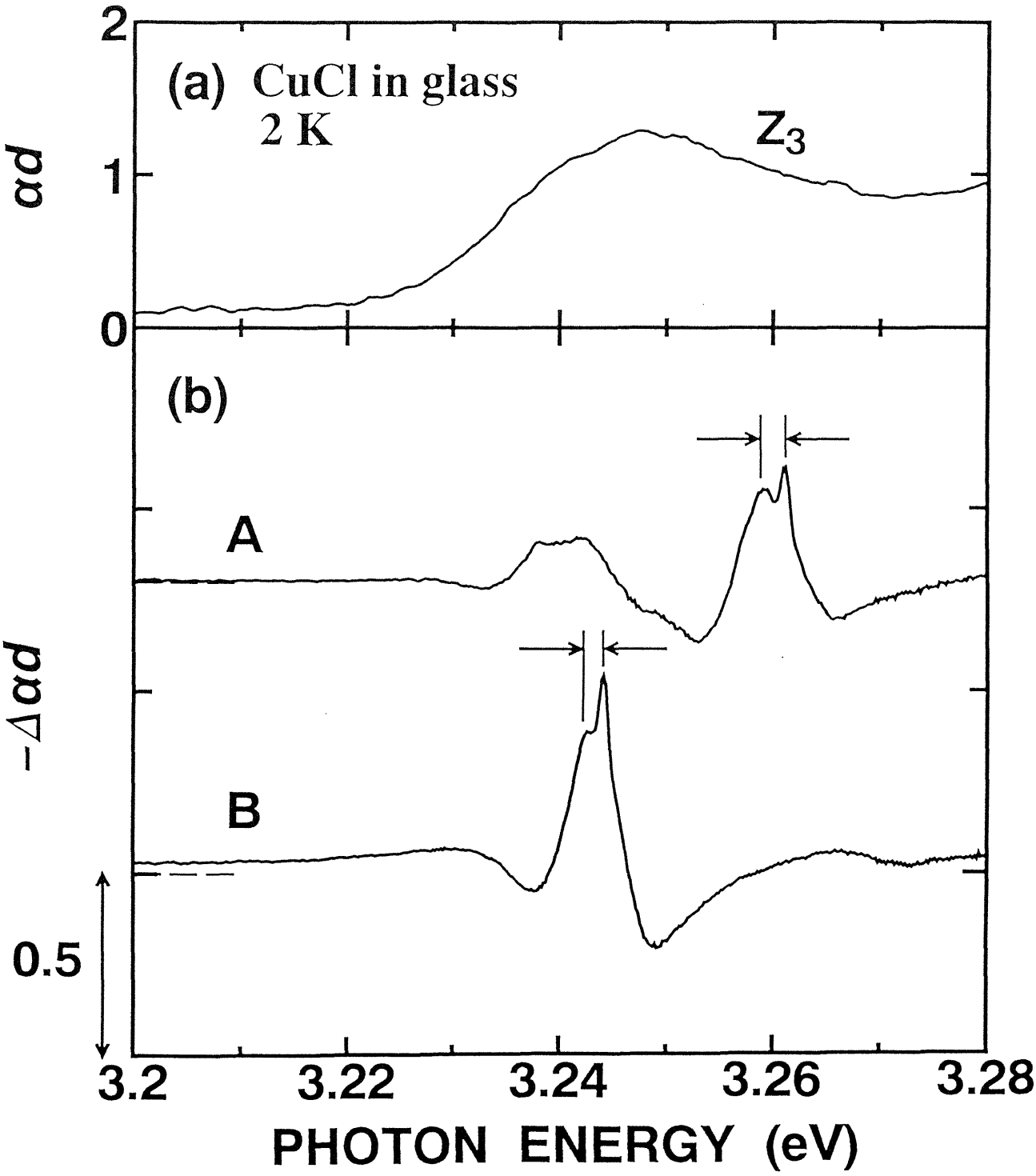
(a) CuCl in glass
2 K
Z_3
αd
(b)
A
B
$-\Delta\alpha d$
0.5
2
1
0
3.2
3.22
3.24
3.26
3.28
PHOTON ENERGY (eV)

Fig. 6.1.1

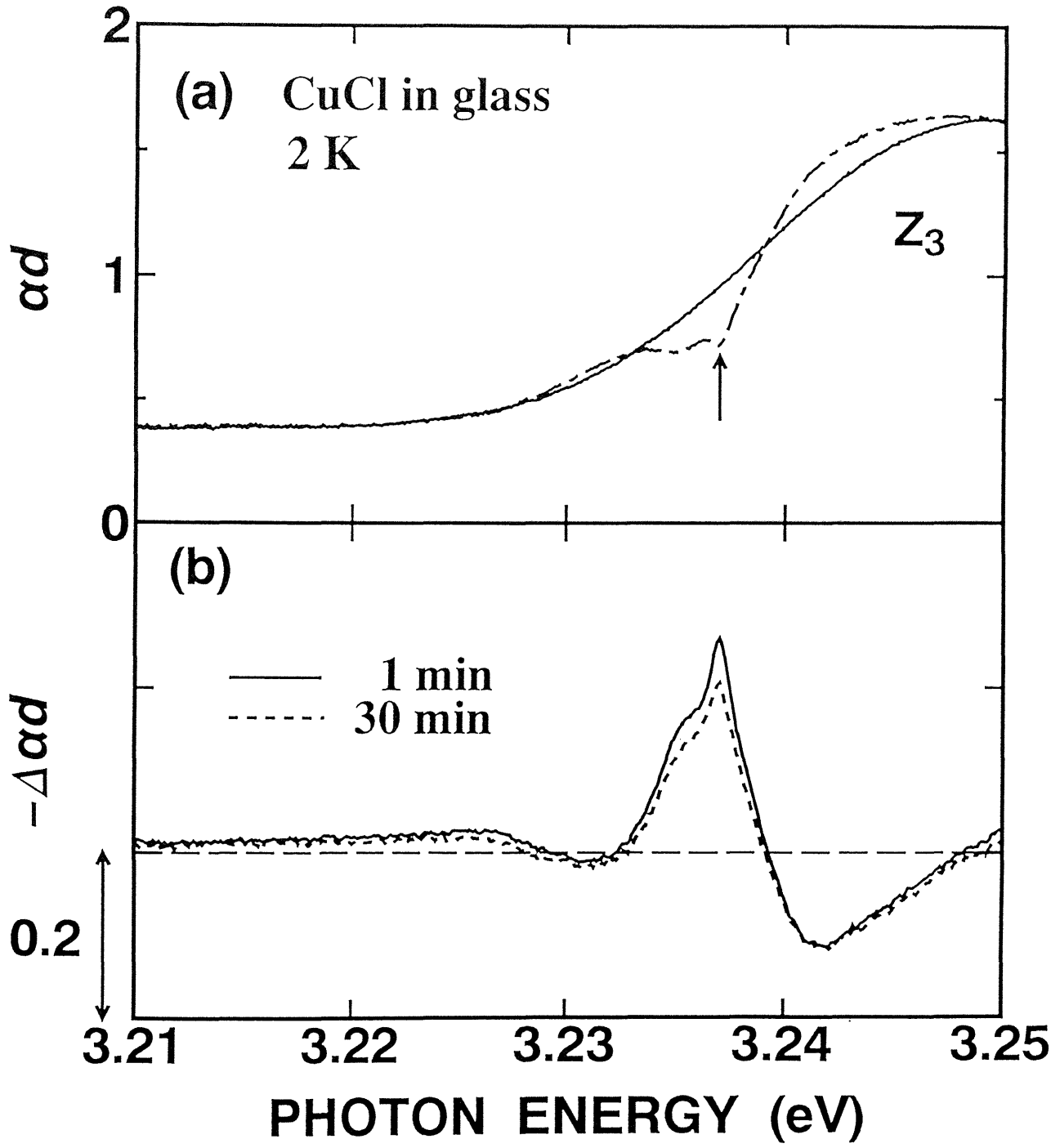
(a) CuCl in glass
2 K
Z_3
αd
2
1
0
(b)
1 min
30 min
$-\Delta\alpha d$
0.2
3.21
3.22
3.23
3.24
3.25
PHOTON ENERGY (eV)

Fig. 6.1.2

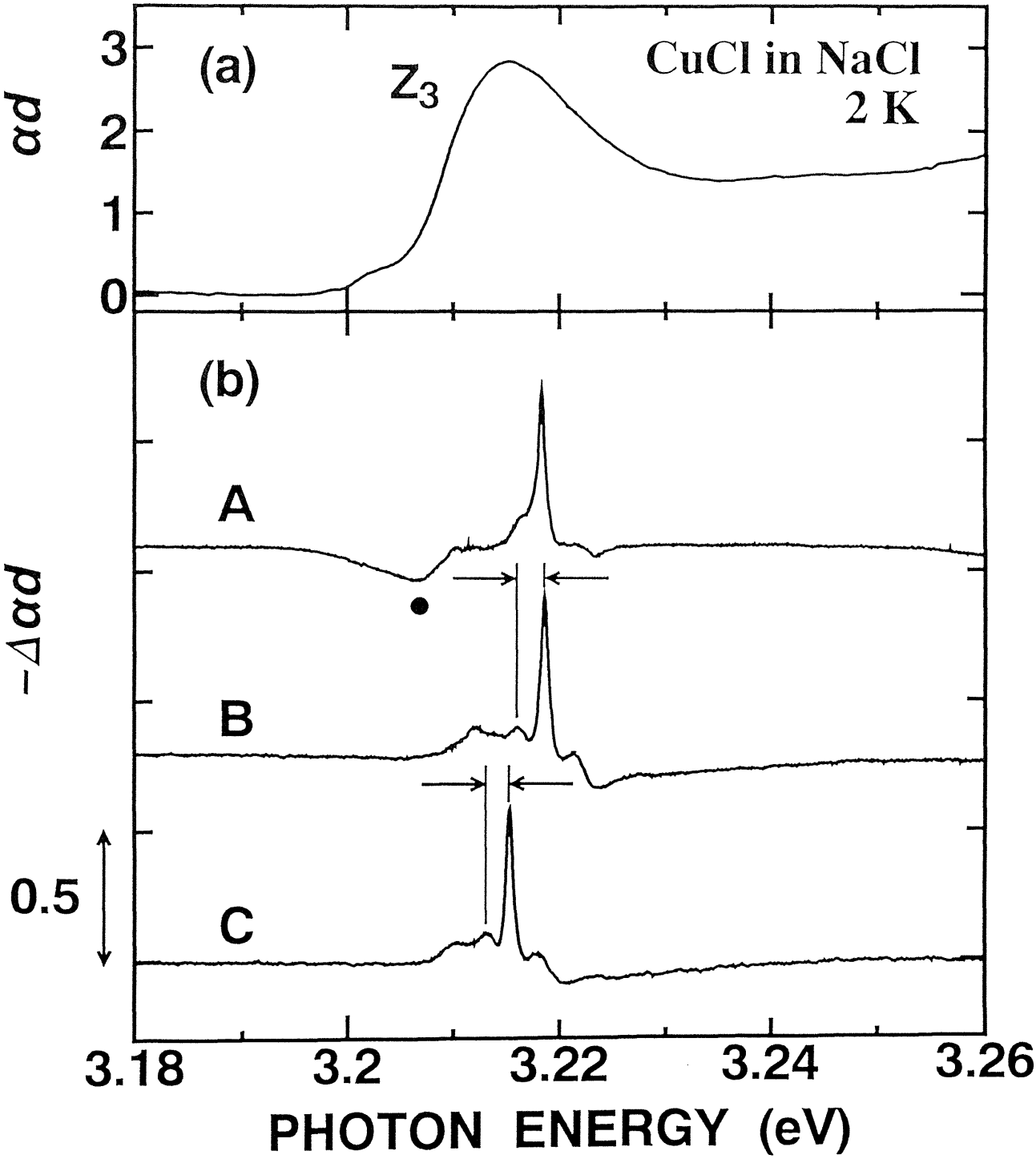
(a)
Z_3
CuCl in NaCl
2 K
αd
3
2
1
0
(b)
A
B
C
$-\Delta\alpha d$
0.5
3.18
3.2
3.22
3.24
3.26
PHOTON ENERGY (eV)

Fig. 6.1.3

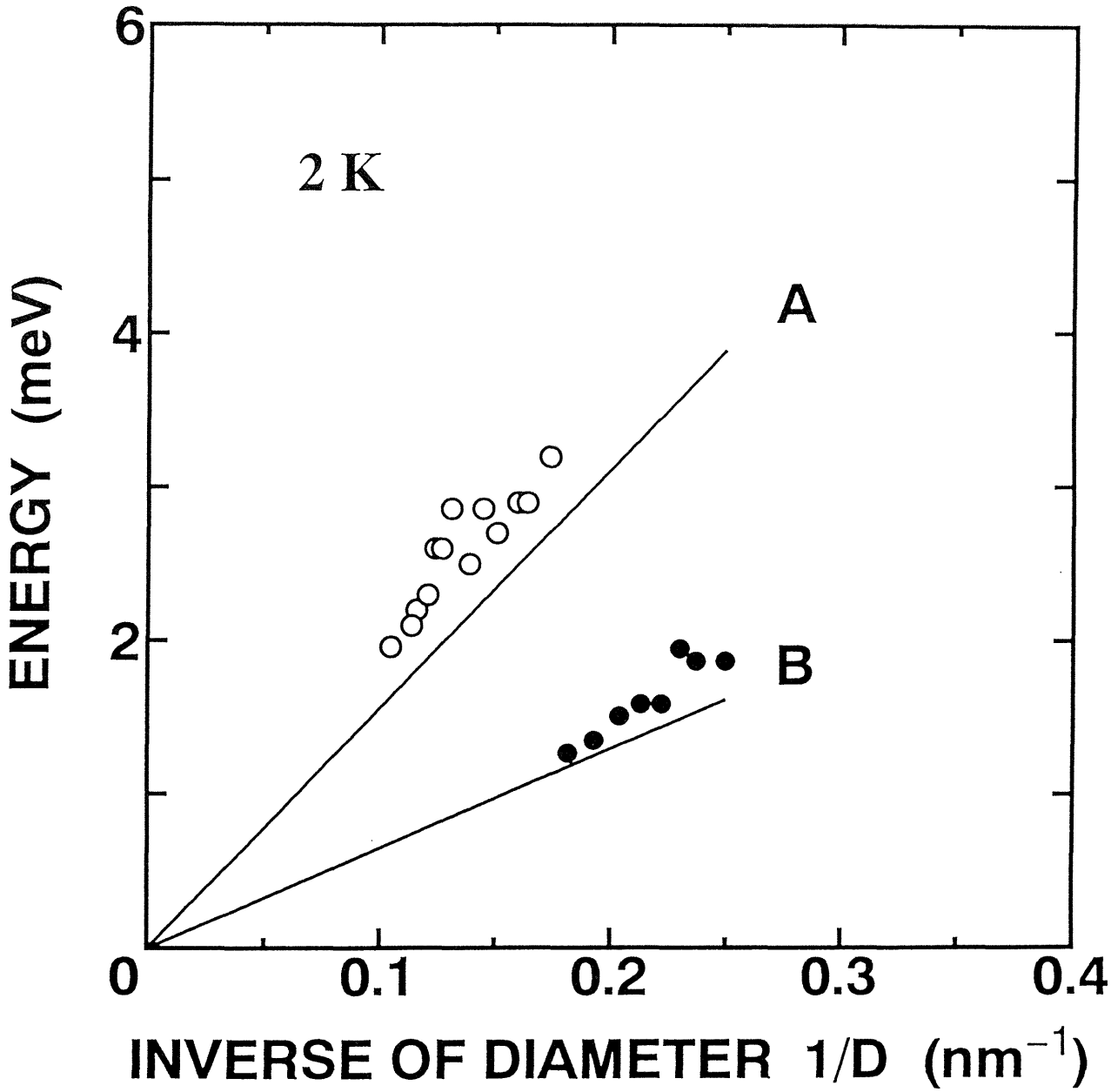

Fig. 6.1.4

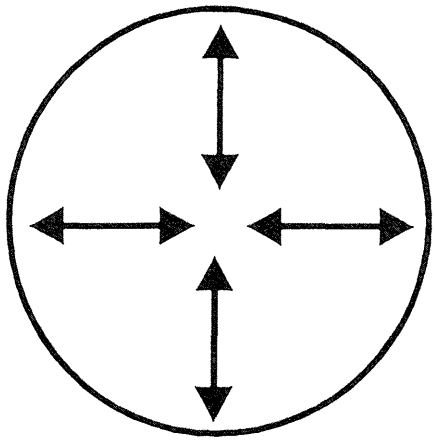

(a)

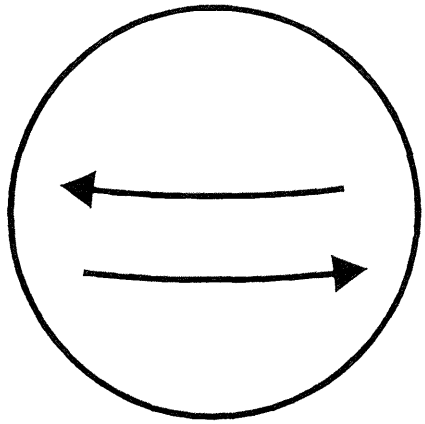

(b)

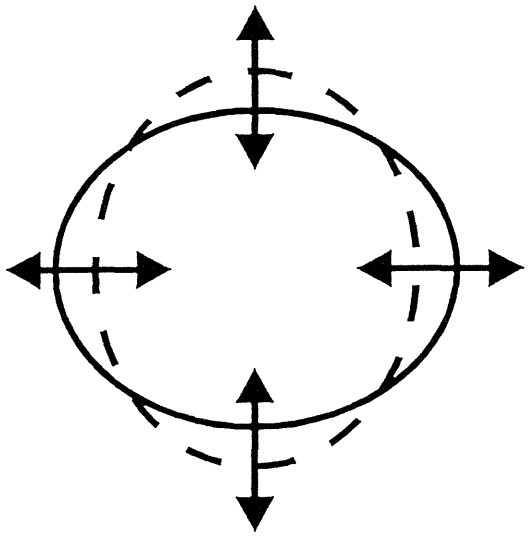

(c)

Fig. 6.1.5

6.2 Observation of Excited States of $Z_{1,2}$- and Z_3-Excitons Confined in CuCl Nanocrystals

In Sec. 6.1, we exhibited the size dependence of acoustic phonons confined in CuCl nanocrystals by using persistent spectral hole-burning (PSHB) phenomena and discussed the matrix dependence of the phonon energies. This suggests that the PSHB phenomena can be applied to size-selective spectroscopies. In fact, the size-selective spectroscopies by using the PSHB phenomena succeeded in observations of 1p-state of Z_3-excitons [1] and charged excitons [2] confined in CuCl nanocrystals. In this section, we discuss higher-excited states of $Z_{1,2}$- and Z_3-excitons confined in CuCl nanocrystals embedded in a NaCl crystal by using the PSHB phenomena. CuCl nanocrystals with a certain size are selectively excited owing to quantum confinement effects [3,4]. A sharp spectral hole and satellite holes are formed in the exciton absorption bands under the site-selective excitation. Not only the higher-energy shifts but also the splittings of the satellite holes are observed as the pump photon energy, *i.e.*, the main-hole energy increases. The splittings are ascribed to the shape of the nanocrystals. Theoretical results on the quantum confinements can explain the splittings.

6.2.1 Experimental Results and Discussions

Figure 6.2.1 shows the hole spectra at various pump photon energies at 20 K. Several peaks are observed not only on the lower-energy side but also on the higher energy side of the main hole. As the pump photon energy decreases, the several peaks denoted by symbols are shifted toward the lower energy side and their energy intervals decrease.

In Fig. 6.2.2, the relations between the hole energies (main-hole energies) and the peak

energies in the hole spectra are plotted by several symbols. Similar peaks due to size-quantized excitons are observed in photoluminescence excitation spectra of CuCl nanocrystals embedded in a NaCl crystal, as is shown in Ref. 3: Assuming the quantum confinements, several sets of exciton parameters including translational masses of Z_3-excitons, Luttinger parameters and k-linear terms are estimated. We will assign the peaks in the hole spectra.

Crosses (×), open circles (○) and open triangles (△) are parallel to solid circles (●; main holes) and considered to be ascribed to the phonon sidebands related to the main holes. Solid lines A to D indicate the selectively-excited 1s Z_3-exciton state, the 1LA (15 meV), 2TO (42 meV) and 2LO (52 meV) phonon sidebands of the main hole, which are in good agreement with the solid circles (●), crosses (×), open circles (○) and open triangles (△) in the hole spectra, respectively.

Dashed lines H and I represent the theoretical results of Z_3-excitons whose quantum number for the confinement, l, are 2 and 3, respectively, on the assumption of the quantum confinements in the nanocrystals: pluses (+) and open diamonds (◇) are in agreement with Z_3-excitons states of l=2 and 3, respectively.

Solid lines E to G represent the theoretical results of light- and heavy-mass $Z_{1,2}$-excitons for the confinement. The splitting of the heavy mass exciton states are ascribed to the sign of the k-linear term in the calculation [3]: solid triangles (▲) are due to the light-mass excitons. A part of open squares (□) and solid squares (■) are in agreement with the line F. Solid diamonds (♦) and a part of open squares (□) are in good agreement with the line E: the peaks indicated by open squares (□), solid squares (■) and solid diamonds (♦) are attributed to the heavy-mass exciton states.

The excited states and the splitting of excitons confined in nanocrystals are observed by using the PSHB phenomena. Thus, the PSHB spectroscopy is useful.

6.2.2 Summary

We study the excited states of excitons of CuCl nanocrystals embedded in a NaCl crystal by means of PSHB spectroscopy. The experimental results of the higher-energy shifts are in good agreement with the site-selective photoluminescence and the theoretical results. Moreover, we observed the satellite-hole splitting ascribed to the exciton confinement in the nanocrystals. This implies that the PSHB spectroscopy is one of the powerful tools to investigate the exciton states in nanocrystals.

References

[1] N. Sakakura and Y. Masumoto, To be published in Jpn. J. Appl. Phys. **36** (1997).

[2] T. Kawazoe and Y. Masumoto, Phys. Rev. Lett. **77**, 4942 (1996).

[3] T. Itoh, Y. Iwabuchi and T. Kirihara, Phys. Status solidi B**146**, 531 (1988).

[4] M. G. Bawendi, W. L. Wilson, L. Rothberg, P. J. Carroll, T. M. Jedju, M. L. Steigerwald and L. E. Brus, Phys. Rev. Lett. **65**, 1623 (1990).

Figure Captions

Fig. 6.2.1. Hole spectra at various pump photon energies at 20 K. The spectra A to D are measured at the pump photon energies of 3.280, 3.263, 3.246 and 3.229 eV, respectively, as indicated by upward arrows. The energy density, the pulse duration, pulse repetition and the excitation period are 64 $\mu J/cm^2$, 5 ns, 30 Hz and 3 min, respectively.

Fig. 6.2.2. Energy relation between the observed main hole and the peaks in the hole spectra of Fig. 6.2.1. Symbols and curves indicated the experimental data and the theoretical results, respectively, which were mentioned in the text. A vertical dashed–line indicates the bulk Z_3– exciton energy. Horizontal arrows indicate the energies of the 1S states of the Z_3– and $Z_{1,2}$– excitons, respectively.

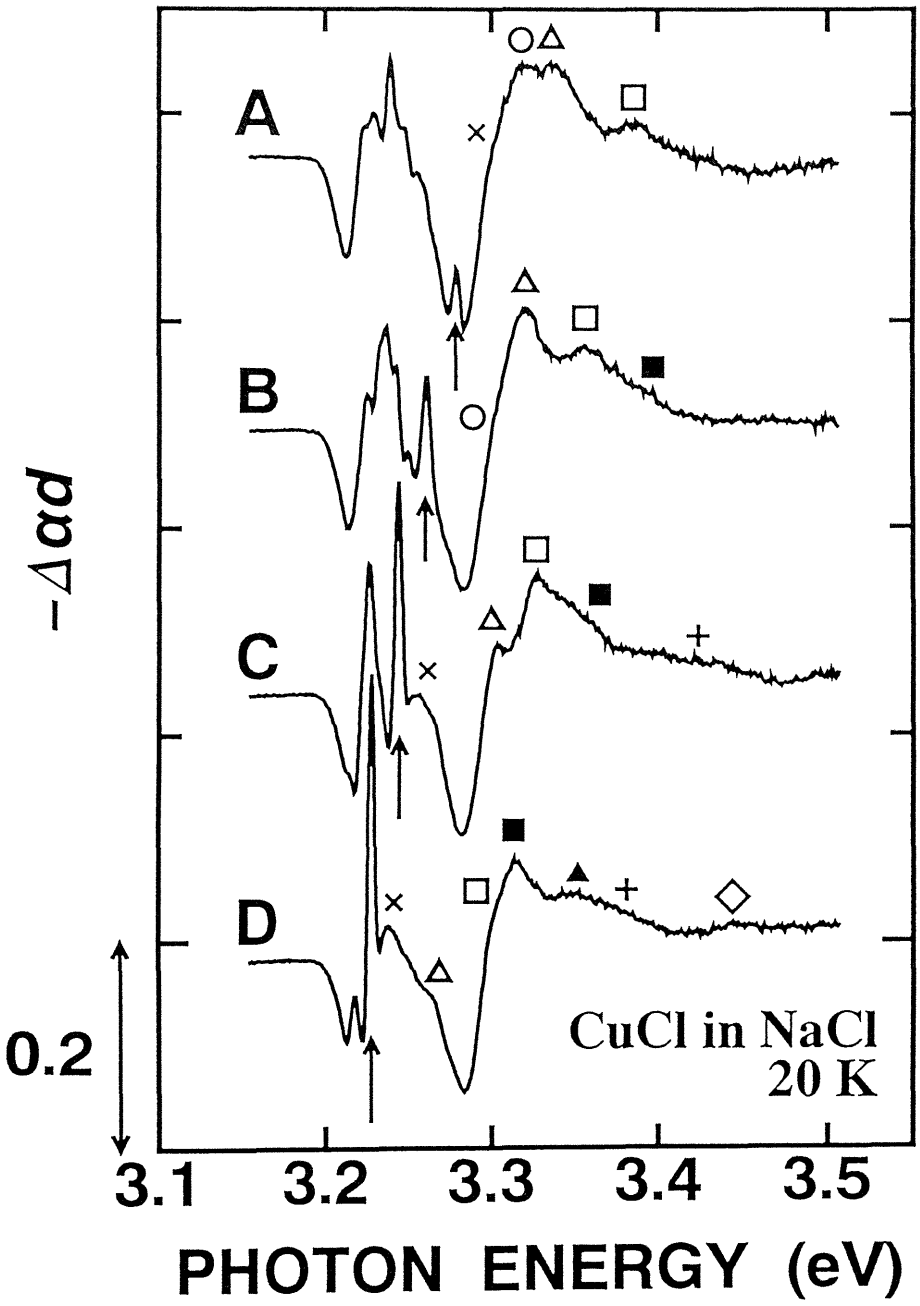
A
B
C
D
$-\Delta\alpha d$
0.2
CuCl in NaCl
20 K
3.1
3.2
3.3
3.4
3.5
PHOTON ENERGY (eV)

Fig. 6.2.1

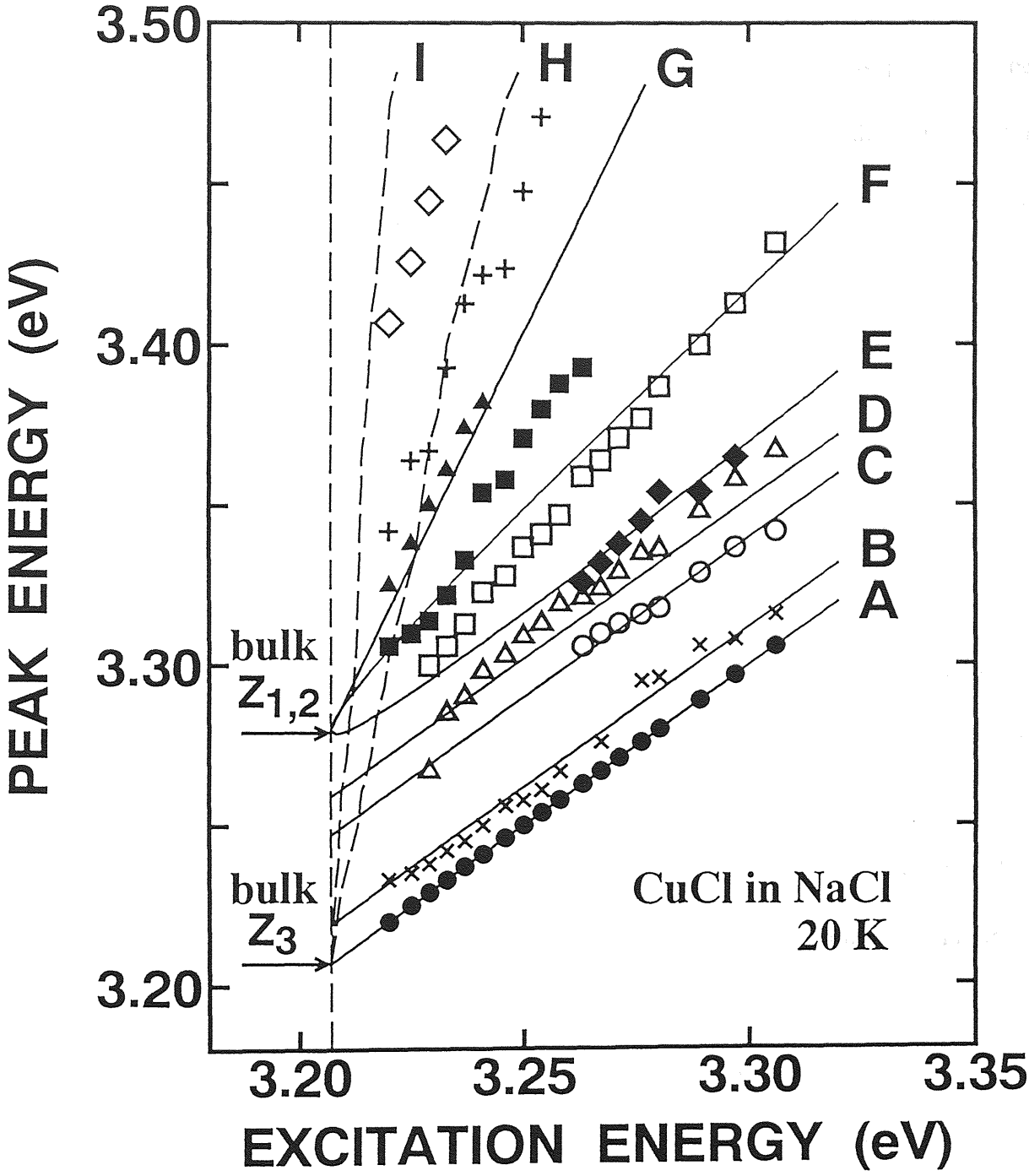
3.50
3.40
3.30
3.20
PEAK ENERGY (eV)
I
H
G
F
E
D
C
B
A
bulk
$Z_{1,2}$
bulk
Z_3
CuCl in NaCl
20 K
3.20
3.25
3.30
3.35
EXCITATION ENERGY (eV)

Fig. 6.2.2

6.3 Demonstration of Frequency-Domain Optical Data Storage (FDOS) by Using CuCl Nanocrystals

In the previous sections, persistent spectral hole-burning (PSHB) has proven to be applicable to size-selective spectroscopies. At the same time, PSHB has the potential for technological applications to frequency-domain optical data storage [1]. This has resulted in engineering and materials research on PSHB.

Conventional recording materials is rotated under an actuator, and a voice-coil moves a recording head in and out along a radius of the rotating disk. Areal storage density is fundamentally limited by optical diffraction. Moreover, such a rotating storage technology suffers from two limitation on access time: latency and search time. Both latency and search time determine the random access performance of this type of data storage.

For future data storage technologies, it is desirable to improve both storage density and data access time. The improvements in both areal density and random access performance can be achieved by using PSHB phenomena. PSHB consists of particular photoinduced changes that can occur within inhomogeneously broadened lines of absorbing centers in solids at low temperatures. In one laser focal volume with a pump photon energy, only one group of absorbing centers are excited, and different groups of centers can be selectively excited by tuning the pump photon energies. Since the photon energies at which holes are burned add a new dimension for addressing data, this type of storage scheme is called "Frequency-domain optical storage (FDOS)".

The idea of using transient saturation spectral holes for data storage was patented by Szabo [2]. In order to realize a direct-access storage device, it is essential to use materials

in which the photoinduced change persists on time scales of months or years, as is often the case with PSHB. The concept of using persistent spectral-holes for FDOS was proposed by Castro *et al* [3].

For realizing PSHB optical memory, we must find out the PSHB materials with a large Debye-Waller factor at high temperature [4]. CuCl nanocrystal systems are found to maintain the spectral holes at high temperature up to 150 K [5] and have the large Debye-Waller factor which is much over 0.5 [6]. Thus, CuCl nanocrystals have a potential for becoming the high temperature PSHB materials. In this section, we demonstrate the frequency-domain optical data storage using CuCl nanocrystal systems.

6.3.1 Experimental Results

Figure 6.3.1 shows three holes burned sequentially in CuCl nanocrystals embedded in aluminoborosilicate glass. The average radius of the nanocrystals is 2.5 nm, determined by the small-angle X-ray scattering. The Z_3-exciton absorption band is inhomogeneously broadened owing to the size distribution. However, we can burn spectral-holes with much narrower linewidth in the Z_3-exciton absorption band under the site-selective excitation. The holes are burned successively from the higher-energy side to the lower-energy side in the absorption band and stored for more than several hours at low temperature. If we define the presence or the absence of a hole correspond to "1" or "0", respectively, we can use CuCl nanocrystals in glass as a binary data storage device.

Similar successive hole formation can be observed in CuCl nanocrystals embedded in a NaCl crystal. Figure 6.3.2 shows the demonstration of frequency-domain optical data

storage by using CuCl nanocrystals embedded in a NaCl single crystal. The spectral holes can be formed sequentially by varying the pump photon energies. In addition, the spectral holes can be erased by the broad-band light irradiation or by the thermal annealing [7]. This implies that the nanocrystal systems can be used as a rewritable optical memory.

6.3.2 Summary

Our discovery of persistent spectral hole-burning phenomena in semiconductor nanocrystal systems implies that the semiconductor nanocrystal systems have the potential for application to an optical data storage device. We demonstrated the optical data storage in CuCl nanocrystals embedded in glass and a NaCl crystal.

References

[1] *Persistent Spectral Hole-Burning: Science and Applications*, edited by W. E. Moerner, (Springer-Verlag, Berlin, 1988) Chap. 7.

[2] A. Szabo, U. S. Patent No. 3,896,420 (1975).

[3] G. Castro, D. Haarer, R. M. Macfarlane and H. P. Trommsdorff, U. S. Patent No. 4,101,976 (1978).

[4] S. Saikan, A. Imaoka, Y. Kanematsu, K. Sakoda, K. Kominami and M. Iwamoto: Phys. Rev. B**41**, 3185 (1990).

[5] S. Okamoto and Y. Masumoto, Jpn. J. Appl. Phys. **34** Suppl. 34-1, 128 (1995).

[6] S. Okamoto and Y. Masumoto, J. Lumin **64**, 253 (1995).

[7] Y. Masumoto, S. Okamoto, T. Yamamoto and T. Kawazoe: Phys. Status Solidi B**188**, 209

(1995).

Figure Captions

Fig. 6.3.1. An example of sequential hole formation of CuCl nanocrystals embedded in aluminoborosilicate glass. The spectra (a) and (b) are the absorption spectrum and the absorption-change spectra of the sample, respectively. The average radius of CuCl nanocrystals is 2.5 nm. The sample at 20 K is irradiated for 3 min by using dye laser pulses with the energy density of 0.09 $\mu J/cm^2$ at three photon energies, 3.2618 eV (1), 3.2533 eV (2) and 3.2448 eV (3), successively. First, spectrum A is measured after the laser exposure at 3.2618 eV. Second, spectrum B is measured after the exposure at 3.2533 eV. Finally, spectrum C is measured after the exposure at 3.2448 eV.

Fig. 6.3.2. An example of sequential hole formation of CuCl nanocrystals embedded in a NaCl host crystal. The spectrum (a) and spectra (b) are the absorption spectrum and the absorption-change spectra, respectively. The average radius of the nanocrystals is 3.5 nm. The sample at 15 K is irradiated for 3 min by using dye laser pulses with the energy density of 4 nJ/cm^2. The pulse duration and pulse repetition are 5 ns and 30 Hz, respectively. First, the spectrum A is measured after the laser exposure at 3.236 eV (1). Second, the spectrum B is measured after the laser exposure at 3.228 eV (2). Third, the spectrum C is measured after the laser exposure at 3.220 eV (3). Finally, the spectrum D is measured after the laser exposure at 3.211 eV (4).

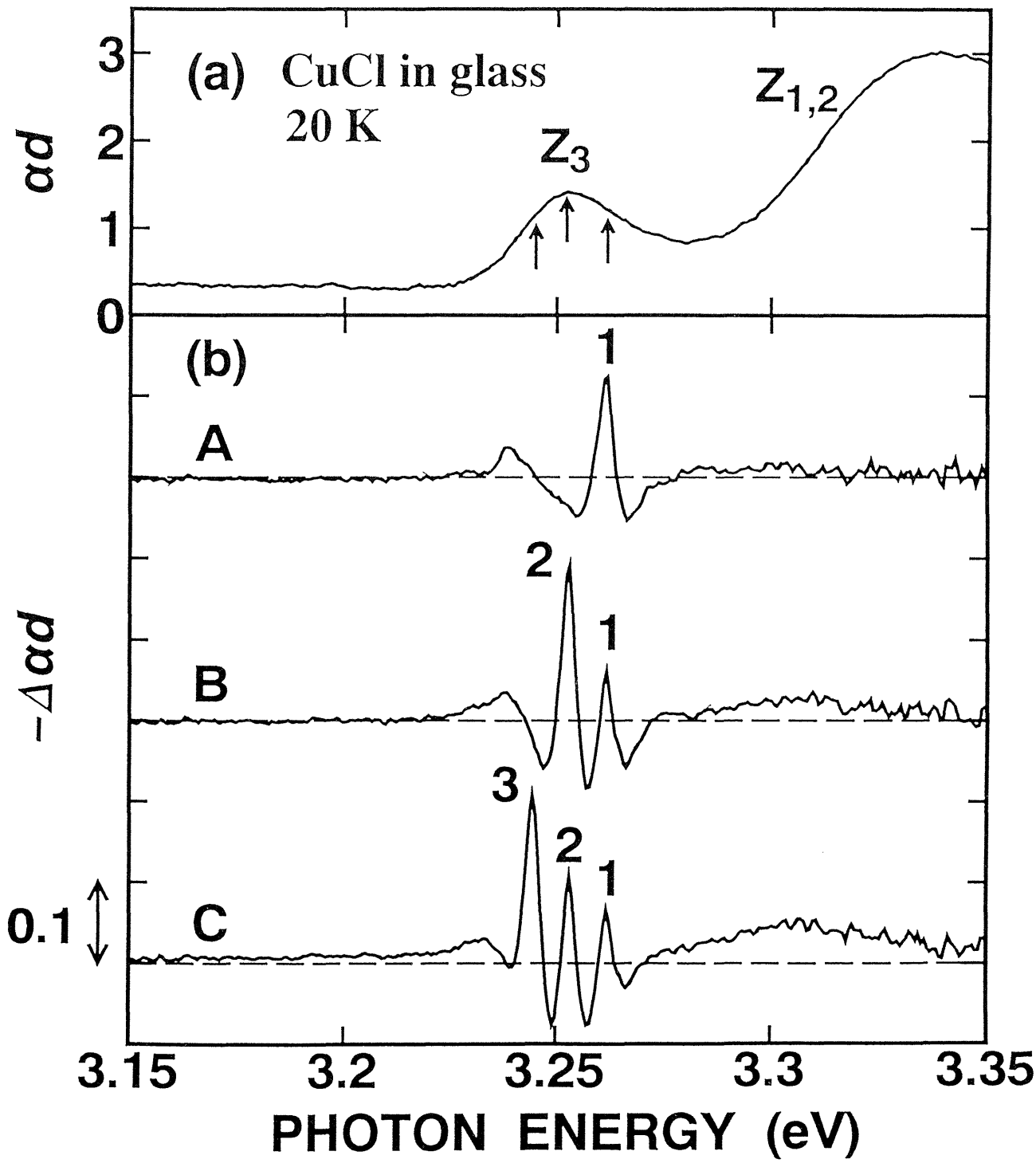
(a) CuCl in glass
20 K
Z_3
$Z_{1,2}$
αd
3
2
1
0
(b)
A
B
C
1
2
1
3
2
1
$-\Delta\alpha d$
0.1
3.15
3.2
3.25
3.3
3.35
PHOTON ENERGY (eV)

Fig. 6.3.1

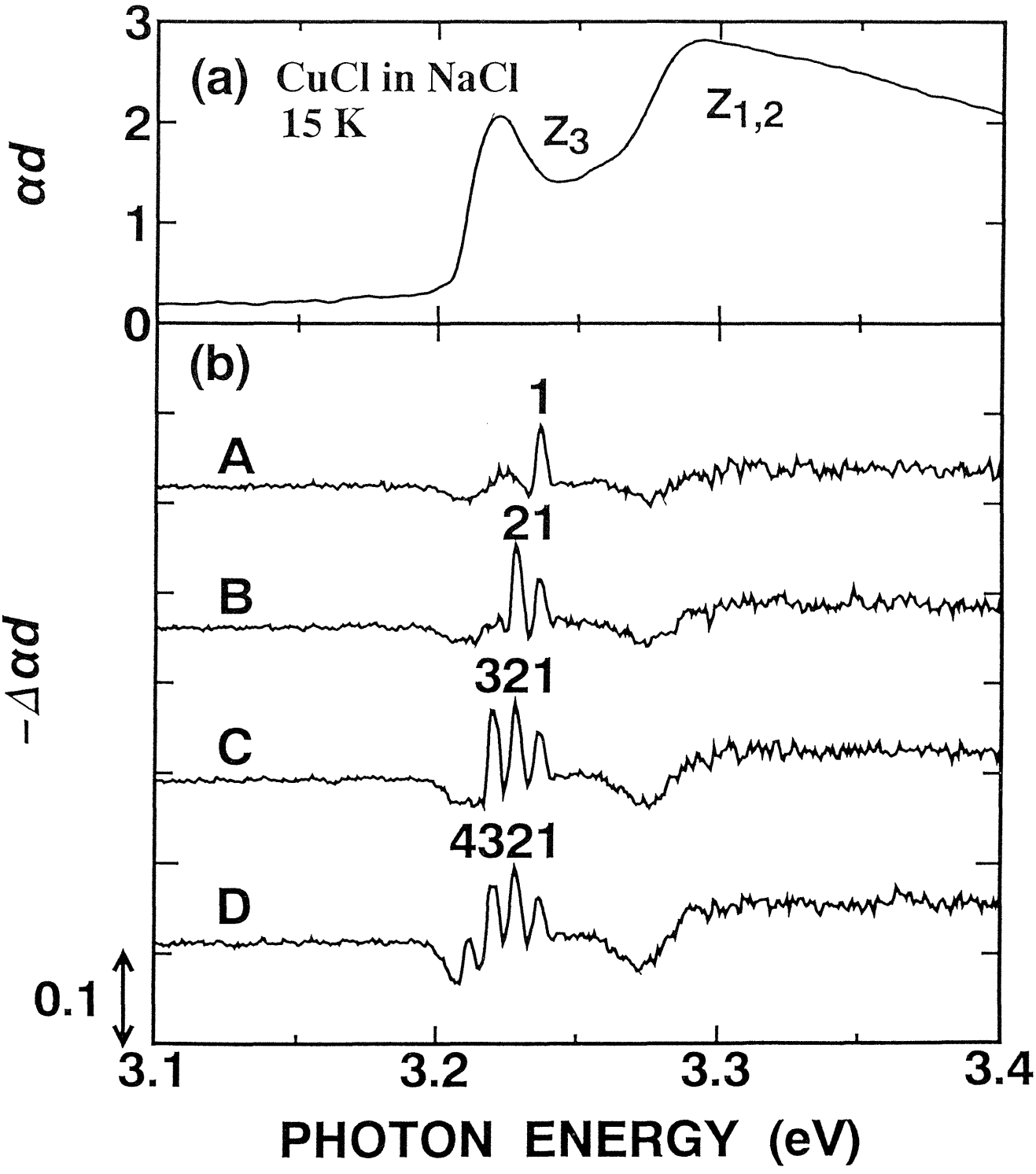
(a) CuCl in NaCl
15 K
Z_3
$Z_{1,2}$
αd
(b)
1
A
21
B
321
C
4321
D
$-\Delta\alpha d$
0.1
3
2
1
0
3.1
3.2
3.3
3.4
PHOTON ENERGY (eV)

Fig. 6.3.2

Chapter VII

Conclusion

We have studied persistent spectral hole-burning (PSHB) phenomena of cuprous chloride (CuCl) nanocrystals. In particular, we focus on two aspects: clarifying mechanisms of the PSHB phenomena and searching for the possibilities of applications of the PSHB phenomena.

In CuCl nanocrystals embedded in a NaCl crystals, we found correlations between the PSHB phenomena and photoluminescence spectral-changes of excitons bound to Cu^+-ion vacancies in CuCl nanocrystals and of Cu^+ dimers in a NaCl crystal. The spectral-changes can be triggered by Cu^+-ion displacements in CuCl nanocrystals and in a NaCl crystal.

On the other hand, in CuCl nanocrystals embedded in aluminoborosilicate glass, the PSHB phenomena are considered to be mainly caused by photophysical mechanisms, *e. g.*, photoinduced structural-changes at nanocrystal-glass interface and/or glass.

PSHB phenomena of the nanocrystals can be applied to the precise, high-resolution spectroscopy for the nanocrystals with a certain size, and to optical storage. We showed some examples of the applications by using the PSHB phenomena: We report on observation of confined acoustic phonons in CuCl nanocrystals. The nanocrystal-size-dependent energy intervals between the zero-phonon line and phonon sidebands in the hole-burning spectra coincide with the calculated energies of confined acoustic phonons in nanometer-size elastic spheres. We conclude that the phonon sidebands are due to confined acoustic phonons in CuCl nanocrystals. The observed confined acoustic phonon mode depends on the surrounding

matrices, glass and NaCl: Surface modes of the acoustic phonons were not observed in case of NaCl matrix, but observed in case of glass matrix. Slight deviation between the experimental and theoretical results is observed. This suggest that the shape of the nanocrystal is not perfectly spherical.

Next, we show the nanocrystal-size-dependence of the higher-excited states of excitons and LO- and TO-phonons confined in CuCl nanocrystals by means of the PSHB phenomena. Moreover, quantum confined exciton-excited-states is observed and in agreement with the theoretical results on the quantum confinements.

PSHB phenomena can also applied to optical data storage. We demonstrate the frequency-domain optical data storage using CuCl nanocrystals.

PSHB phenomena are observed in various semiconductor nanocrystal systems. We believe that the PSHB phenomena become a powerful tool to investigate single nanocrystals of various semiconductors and will apply to frequency-domain optical data storage.

Acknowledgements

This research has been carried out under the supervision of Prof. Yasuaki Masumoto's. The author wishes to express his sincere thanks to Prof. Yasuaki Masumoto of University of Tsukuba for his useful discussions and instructions.

The author also wishes to express his sincere thanks to Dr. Yoshihiko Kanemitsu of University of Tsukuba for his encouragement and comments. He wishes to acknowledge to Dr. Tomobumi Mishina and Dr. Tsuyoshi Okuno of University of Tsukuba for valuable advice and discussions.

The author would like to express deeply thanks to Dr. Lev G. Zimin for sample preparations and fruitful discussions.

The experiments of small angle X-ray scattering had proceeded at The National Laboratory for High Energy Physics (KEK). The author is indebted to Prof. Y. Amemiya of KEK for his kind help.

Finally, the author is grateful to other members of the group under Prof. Masumoto for their kind help and encouragements.

List of Publications

1. "**Persistent spectral hole burning in semiconductor microcrystals**",
   Yasuaki Masumoto, Lev. G. Zimin, Kazuhiko Naoe, Shinji Okamoto and Toshihiro Arai,
   Mater. Sci. Eng. B**27**, L5 (1994).

2. "**Observation of persistent spectral hole-burning in semiconductor nanocrystals**",
   Yasuaki Masumoto, Lev G. Zimin, Kazuhiko Naoe, Shinji Okamoto, Tadashi Kawazoe and Tetsuya Yamamoto,
   J. Lumin. **64**, 213 (1995).

3. "**Persistent spectral hole-burning phenomenon of semiconductor quantum dots**",
   Yasuaki Masumoto, Shinji Okamoto, Tetsuya Yamamoto and Tadashi Kawazoe,
   Phys. Status Solidi B**188**, 209 (1995).

4. "**Persistent spectral hole-burning in CuCl nanocrystals: Demonstration of optical data storage**",
   Shinji Okamoto and Yasuaki Masumoto,
   Jpn. J. Appl. Phys. **34**, Suppl. **34-1**, 128 (1995).

5. "**Observation of confined acoustic phonons in semiconductor nanocrystals by means of the persistent spectral hole-burning spectroscopy**",

Shinji Okamoto and Yasuaki Masumoto,

J. Lumin. **64**, 253 (1995).

6. "**Persistent hole-burning spectroscopy of CuCl microcrystallites: Host-matrix -dependence on the hole-burning effects**",

Shinji Okamoto and Yasuaki Masumoto,

Technical Digest of CLEO/Pacific Rim '95, pp. 260 (1995).

7. "**Demonstration of frequency-domain optical data storage of CuCl semiconductor nanocrystal systems**",

Shinji Okamoto and Yasuaki Masumoto,

Jpn. J. Appl. Phys. **35**, 512 (1996).

8. "**Persistent spectral hole-burning of CuCl quantum dots**",

Shinji Okamoto and Yasuaki Masumoto,

Mater. Res. Soc. Symp. Proc. **405**, 301 (1996).

Other Fields

1. "**Biexciton binding energy in CuCl quantum dots**",

Yasuaki Masumoto, Shinji Okamoto and Satoshi Katayanagi,

Phys. Rev. B**50**, 18658 (1994).

2. "**Third-order nonlinear optical susceptibility and photoluminescence in porous silicon**",

Yoshihiko Kanemitsu, Shinji Okamoto and Akihiro Mito,

Phys. Rev. B**52**, 10752 (1995).

3. "**Photoluminescence properties of surface-oxidized Ge and Si nanocrystals**",

Yoshihiko Kanemitsu and Shinji Okamoto,

Proceedings of the 23rd International Conference on the Physics of Semiconductors, edited by M. Scheffler and R. Zimmermann (world Scientific, Singapore 1996), p.1625.

4. "**Quantum confinement effects on photoluminescence from silicon single quantum wells**",

Shinji Okamoto, Yoshihiko Kanemitsu and Yasuaki Masumoto,

Proceedings of the 23rd International Conference on the Physics of Semiconductors, edited by M. Scheffler and R. Zimmermann (world Scientific, Singapore 1996), p.1863.